

# The $E_{\text{p},\text{i}} - E_{\text{iso}}$ correlation: type I gamma-ray bursts and the new classification method

P. Y. Minaev,<sup>1,2\*</sup> A. S. Pozanenko,<sup>1,2,3</sup>

<sup>1</sup> Space Research Institute of the Russian Academy of Sciences (IKI), 84/32 Profsoyuznaya Str., Moscow, 117997, Russia

<sup>2</sup> Moscow Institute of Physics and Technology (MIPT), 9 Institutskiy per., Dolgoprudny, 141701, Russia

<sup>3</sup> National Research University Higher School of Economics, Moscow, 101000, Russia

Accepted XXX. Received YYY; in original form ZZZ

## ABSTRACT

We present the most extensive sample of 45 type I (short) and 275 type II (long) gamma-ray bursts (GRB) with known redshift to investigate the correlation between the rest frame peak energy,  $E_{\text{p},\text{i}}$  and the total isotropic equivalent energy,  $E_{\text{iso}}$  of the prompt emission (Amati relation). The  $E_{\text{p},\text{i}} - E_{\text{iso}}$  correlation for type I bursts is found to be well-distinguished from the one constructed for type II bursts and has a similar power-law index value,  $E_{\text{p},\text{i}} \sim E_{\text{iso}}^{0.4}$ , which possibly indicates the same emission mechanism of both GRB types. We show that the initial pulse complex (IPC) of type I bursts with an extended emission and regular type I bursts follow the same correlation. We obtain similar results for type II bursts associated with Ic supernovae and for regular type II bursts. Three possible outliers from the  $E_{\text{p},\text{i}} - E_{\text{iso}}$  correlation for type II subsample are detected. Significant evolution of the  $E_{\text{p},\text{i}} - E_{\text{iso}}$  correlation with redshift for type II bursts is not found. We suggest the new classification method, based on the  $E_{\text{p},\text{i}} - E_{\text{iso}}$  correlation and introduce two parameters,  $EH = E_{\text{p},\text{i},2} E_{\text{iso},51}^{-0.4}$  and  $EHD = E_{\text{p},\text{i},2} E_{\text{iso},51}^{-0.4} T_{90,\text{i}}^{-0.5}$ , where  $E_{\text{p},\text{i},2}$  is the value of  $E_{\text{p},\text{i}}$  parameter in units of 100 keV,  $E_{\text{iso},51}$  is the value of  $E_{\text{iso}}$  parameter in units of  $10^{51}$  erg and  $T_{90,\text{i}}$  is the rest frame duration in units of seconds.  $EHD$  is found to be the most reliable parameter for the blind type I / type II classification, which can be used to classify GRBs with no redshift.

**Key words:** transients: gamma-ray bursts – transients: supernovae – catalogues – methods: data analysis – methods: statistical

## 1 INTRODUCTION

Two classes of gamma-ray bursts (GRB) were discovered in a series of KONUS experiments forty years ago (Mazets et al. 1981) and later confirmed in the Phebus/GRANAT experiment (Dezalay et al. 1992). The classification scheme based on the bimodal nature of the duration distribution with the separation at  $T_{90} \sim 2$  s was proposed in the BATSE/CGRO experiment, where  $T_{90}$  parameter (time interval with integrated counts raise from 5% to 95%) was introduced (Kouveliotou et al. 1993). Type I (short) bursts were also found to have a harder energy spectrum (e.g., in terms of a hardness ratio – the ratio of energy fluxes in different energy bands) and less distinct spectral evolution (lag) comparing with type II (long) ones (Kouveliotou et al. 1993; Norris et al. 2005; Minaev et al. 2010a,b, 2012, 2014).

$T_{90}$  and hardness ratio distributions, used for the classi-

fication of GRBs traditionally, are overlapped significantly. It makes the problem of correct blind classification still very actual, especially in the new era of gravitational wave astronomy. The one and only confirmed gamma-ray burst for the moment, associated with gravitational waves, GRB 170817, is placed in the middle of the overlap region (Abbott et al. 2017a,b; Goldstein et al. 2017; Pozanenko et al. 2018).

Moreover,  $T_{90}$  parameter is highly affected by the number of selection effects. Firstly, it depends on an energy range used for the calculation: a pulse narrowing with an energy follows a power-law with the index of  $\sim -0.4$  (e.g. Fenimore et al. 1995; Minaev et al. 2010b). The energy range used for  $T_{90}$  calculation varies with experiments: (15, 150) keV range is typical for Swift, (10, 1000) keV – for Fermi, and (80, 1200) keV – for Konus-Wind. The pulse narrowing with the energy leads to shifting of  $T_{90}$  separation line, used for a blind classification, with energy range (Minaev et al. 2010b). Additionally,  $T_{90}$  depends on the detector sensitivity and, in particular, on background variations (brighter events with

\* E-mail: minaevp@mail.ru

a stable background are longer). Next, the observed duration depends on redshift of the source  $T_{90} = T_{90,i}(1+z)$ , where  $T_{90,i}$  is the intrinsic (rest-frame) duration. Finally, the energy range used for  $T_{90}$  calculation is shifted to lower energies from the one in the rest frame. All these effects make an estimation of the “true” (not biased)  $T_{90,i}$  value virtually impossible. Therefore,  $T_{90,i}$  values should be used in the analysis with caution, meaning the classification of GRBs based only on their duration is unreliable.

Apart from the duration and spectral hardness, the spectral lag, a parameter characterizing the spectral evolution, was used to classify GRBs: type I bursts have negligible lags while larger positive spectral lags are characteristic of type II GRBs (e.g. Yi et al. 2006; Norris & Bonnell 2006; Zhang et al. 2006; Minaev et al. 2012, 2014). An empirical correlation of the lag on luminosity has been detected for the class of type II GRBs (e.g. Norris et al. 2000; Norris 2002; Gehrels et al. 2006; Schaefer 2007; Hakkila et al. 2008; Ukwatta et al. 2012; Bernardini et al. 2015). Hakkila & Preece (2011); Minaev et al. (2014) showed that the observed properties of short pulses in type II GRBs with a complex multipulse structure are similar to those of type I GRBs. Minaev et al. (2014) also revealed that the lag value is strongly affected by superposition effects in multipulsed bursts: one can obtain negligible lag even for long type II GRB, if it is characterized by a complex structure of light curve. Therefore, at this stage we would ignore the spectral lags as classification indicators. More parameters useful for classification are also discussed e.g. in Donaghy et al. (2006); Berger (2014). One more evident criterion can be added, the detection of kilonova emission for type I bursts (e.g. Jin et al. 2016; Yang et al. 2015; Tanaka 2016; Pozanenko et al. 2018; Pandey et al. 2019).

The correct classification is crucial for understanding GRB progenitors. Type I bursts are associated with a merger of compact binaries, consisted of two neutron stars (Blinnikov et al. 1984; Paczynski 1986; Meszaros & Rees 1992; Rosswog & Ramirez-Ruiz 2003), which was recently confirmed by the gravitational wave experiments LIGO-Virgo for GRB 170817A (Abbott et al. 2017a,b; Goldstein et al. 2017; Savchenko et al. 2017; Pozanenko et al. 2018). Several type I bursts are also accompanied by an additional component with a duration of tens of seconds and a soft energy spectrum – the extended emission (EE), which was detected both in the light curves of several individual events and in the averaged light curve of a group of events (Lazzati et al. 2001; Connaughton 2002; Montanari et al. 2005; Gehrels et al. 2006; Minaev et al. 2010a,b; Norris et al. 2010). The nature of the extended emission is still unclear, it could be related to an activity of a magnetar formed in a merger process (Metzger et al. 2008), beginning of an afterglow (Minaev et al. 2010a), fallback accretion (Rosswog 2007; Barkov & Pozanenko 2011; Gibson et al. 2017). The extended emission sufficiently complicates the GRB classification, confirming that the classification based on the only  $T_{90}$  value is not robust.

Type II bursts are associated with a core collapse of supermassive stars (e.g. Woosley (1993); Paczyński (1998); Mészáros (2006)),  $\sim 10\%$  of type II GRBs with an identified optical component and a measured redshift are also accompanied by a bright (intrinsically) Ic supernovae (e.g. Galama et al. (1998); Hjorth et al. (2003); Paczyński (1998); Kulkarni et al. (1998); Cano et al. (2017); Volnova et al. (2017)). It is unclear, whether the supernova (SN) is the common feature of all type II bursts and its non-detection is connected with only selection effects for the large sample of bursts (supernovae are harder to detect at higher redshift).

Gamma-ray bursts are characterized by a number of correlations between different observational parameters. One can mention hardness – peak flux ( $E_p - f_p$ ) and hardness – fluence ( $E_p - F_{tot}$ ) correlations (e.g. Mallozzi et al. (1995); Dezalay et al. (1997); Lloyd et al. (2000)), which were found in the epoch, when distances to GRB sources were not known. The hardness indicator, spectral parameter  $E_p$  is the position of the extremum (maximum) of the energy spectrum  $\nu F_\nu$ . Later, when the era of optical observations with successful redshift measuring began, these correlations were transformed to intrinsic hardness – peak luminosity ( $E_{p,i} - L_{iso}$ ) and intrinsic hardness – total energy ( $E_{p,i} - E_{iso}$ ) correlations, also known as Yonetoku and Amati relations, respectively (e.g. Yonetoku et al. (2004); Amati et al. (2002)).  $E_{iso}$  ( $L_{iso}$ ) is the isotropic equivalent total energy (peak luminosity), emitted in gamma-rays in (1, 10000) keV range,  $E_{p,i}$  is the intrinsic peak energy,  $E_{p,i} = E_p(1+z)$ . Observed in many cases, break in afterglow light curves confirmed the jet-like non-isotropic emission behavior of GRBs and the necessity of  $E_{iso}$  correction to estimate the collimated energy release  $E_\gamma = E_{iso}(1 - \cos \theta_{jet})$  and collimated luminosity  $L_\gamma = L_{iso}(1 - \cos \theta_{jet})$ , where  $\theta_{jet}$  is the jet opening angle, derived from the time of the afterglow jet break. The hardness – collimation corrected energy ( $E_{p,i} - E_\gamma$ ) correlation was also found, known as Ghirlanda relation (e.g. Ghirlanda et al. 2004).

We investigate the  $E_{p,i} - E_{iso}$  correlation (Amati relation). Previously it was analyzed mostly for type II bursts (e.g. Amati et al. 2002; Amati 2006; Tsvetkova et al. 2017). Type I bursts were found to be outliers of the  $E_{p,i} - E_{iso}$  correlation for type II bursts, so the correlation could also be used for the classification of GRBs (e.g. Lü et al. 2010; Zhang et al. 2012; Qin & Chen 2013; Zhang et al. 2018b; Shahmoradi & Nemiroff 2015; Zou et al. 2018; Pozanenko et al. 2018). More over, in Pozanenko et al. (2019b) the Amati relation was used to estimate the  $E_{p,i}$  value for the second LIGO/Virgo event S190425z connected with binary neutron star merger, which was observed in gamma-ray domain by SPI-ACS/INTEGRAL experiment. Hardness – fluence ( $E_p - F_{tot}$ ) correlation, constructed for GRBs with no redshift, also demonstrated bimodal nature (e.g. Ghirlanda et al. 2009). The sample of investigated type I bursts with measured redshift  $E_{p,i}$  and  $E_{iso}$  parameters was limited in most previous works by  $\sim 20$  events or even less (e.g. Lü et al. 2010; Qin & Chen 2013; Tsvetkova et al. 2017; Pozanenko et al. 2018), making the behavior of the correlation for type I bursts to be unresolved. The sample of type I bursts in Zhang et al. (2018b) reached 31 events and indicated the same value of power-law index of the Amati relation for both type I and type II classes.

The nature of the  $E_{p,i} - E_{iso}$  correlation is unknown. In the trivial case, it could be connected with strong selection effects. One of the probable explanations considers viewing angle effects: the smaller the angle between the observer’s line of sight and the jet axis is, the brighter and harder the gamma-ray emission will be. Under the assumption, the correlation is  $E_{p,i} \sim E_{iso}^{1/3}$  if it is a cone relativistic

**Table 1.** The number of GRBs, depending on experiments used for  $E_{iso}$ ,  $E_{p,i}$  and  $T_{90,i}$  calculation.

Experiment	Type I	Type II	Total	$R^a$
Konus-Wind	12	157	169	0.07
BeppoSAX	0	4	4	0
BATSE/CGRO	0	2	2	0
HETE-2	1	11	12	0.08
Swift	17	67	84	0.20
Fermi	15	34	49	0.31
Total	45	275	320	0.14

<sup>a</sup> -  $R = \text{Type I} / \text{Total}$

jet emission (e.g. Eichler & Levinson 2004; Levinson & Eichler 2005; Pozanenko et al. 2018). So the observable behavior of the correlation could reveal some features of an emission mechanism and a structure of the jet, which is substantial when comparing two types of GRB progenitors. Recently it was shown that the Yonetoku relation (the  $E_{p,i} - L_{iso}$  correlation) also can be explained by the viewing angle effects (Ito et al. 2019).

In the paper, we construct the sample of 45 type I and 275 type II gamma-ray bursts with known redshift and well constrained  $E_p$  and analyze its features, including various selection effects (Section 2). We investigate the  $E_{p,i} - E_{iso}$  correlation for different subsamples (Section 3) and suggest the new classification method of GRBs, introducing two parameters ( $EH = E_{p,i,2} E_{iso,51}^{-0.4}$  and  $EHD = E_{p,i,2} E_{iso,51}^{-0.4} T_{90,i}^{-0.5}$ ), to make the blind classification of the bursts more robust (Section 4).

## 2 THE SAMPLE

### 2.1 The sample construction

To construct the sample of gamma-ray bursts with a measured redshift (both spectroscopic and photometric) and  $E_p$  parameters we used different sources:

1. GRB catalogs of Konus/Wind (Svinkin et al. 2016a; Tsvetkova et al. 2017), BeppoSAX (Frontera et al. 2009), GBM/Fermi (Narayana Bhat et al. 2016) experiments;
2. Papers concerning  $E_{p,i} - E_{iso}$  correlation investigation (e.g. Amati (2006); Qin & Chen (2013); Zhang et al. (2018b); Zou et al. (2018));
3. Papers concerning analysis of individual GRBs (e.g. Minaev & Pozanenko (2017); Pozanenko et al. (2018); Pandey et al. (2019));
4. GCN circulars archive <sup>1</sup>;
5. Online catalog of well-localized GRBs <sup>2</sup>;
6. The catalog of GRB associated supernova (Cano et al. 2017);
7. The paper related to the extended emission investigation of type I GRBs (Norris et al. 2010).

We also derive  $E_{iso}$  and  $E_{p,i}$  values for 45 GRBs using spectral parameters and redshift, available in the literature. The  $E_{iso}$  parameter is calculated via  $E_{iso} = \frac{4\pi D_L^2 F}{1+z}$ , where

<sup>1</sup> [https://gcn.gsfc.nasa.gov/gcn3\\_archive.html](https://gcn.gsfc.nasa.gov/gcn3_archive.html)

<sup>2</sup> <http://www.mpe.mpg.de/~jcg/grbgen.html>

$F$  is the burst fluence in (1, 10000) keV energy range in the rest frame and  $D_L$  is the luminosity distance calculated using standard cosmological parameters,  $H_0 = 67.3 \text{ km s}^{-1} \text{ Mpc}^{-1}$ ,  $\Omega_M = 0.315$ ,  $\Omega_\Lambda = 0.685$  (Planck Collaboration et al. 2014).  $E_{p,i}$  parameter is calculated via  $E_{p,i} = E_p(1+z)$ . The duration of a burst in the rest frame is calculated as  $T_{90,i} = T_{90}/(1+z)$ .

The complete sample of GRBs including 45 type I and 275 type II bursts registered up to 2019, January is presented in Appendix, Table A. 3 type I bursts and 13 type II bursts have photometric redshift estimation. 11 type I bursts are characterized by an extended emission (EE) component, 40 type II bursts are associated with Ic supernova (19 photometrical and 21 spectroscopical ones). For type I+EE bursts we use  $T_{90,i}$ ,  $E_{p,i}$  and  $E_{iso}$  values obtained for the initial pulse complex (IPC) only, ignoring an extended emission component, probably having a different nature. We do not perform any classification analysis at this step and use the classification results from the literature, usually obtained from the complex of different criteria.

The Table 1 summarizes the statistics of the experiments used for calculation  $E_{iso}$  and  $E_{p,i}$  values.  $R$  parameter is defined as the ratio Type I / Total and indicates the utility of the experiment for a classification. The Konus-Wind experiment has been operated since 1994, has a good design (wide energy range, crucial for  $E_{p,i}$  determination, in particular) and, as a consequence, it is the “leading” experiment in our sample (169 GRBs,  $R = 0.07$ ). To maximize the homogeneity of the sample we use the Konus-Wind derived observational parameters in case of GRBs, registered by several experiments (e.g., also by Fermi or Swift). Swift (84 GRBs,  $R = 0.20$ ) is a perfect instrument for a fast and precise localization of GRBs, which is crucial for optical observations and redshift determination; but its capability to measure the  $E_p$  value is limited due to the soft and narrow energy range of the BAT instrument. Fermi (49 GRBs,  $R = 0.31$ ) can not provide a precise localization, but it is excellent for the precise  $E_{p,i}$  determination, complementing the Swift.

### 2.2 Features of the sample

The dependence of  $T_{90,i}$ ,  $E_{iso}$  and  $E_{p,i}$  parameters on redshift for both GRB types and their subsamples is presented at Fig. 1. The corresponding statistics is summarized in Table 2. We also form five equal subsamples of type II bursts (55 bursts each), based on  $z$  values: the  $z_1$  subsample represents the closest bursts while the  $z_5$  one - the most distant bursts. We use them to check the evolution of  $E_{p,i} - E_{iso}$  correlation with redshift (Section 3.4).

#### 2.2.1 Redshift, $z$

Type I bursts are significantly closer than type II ones: the median values are  $z = 0.46$  and  $z = 1.60$ , respectively. Firstly, it should be connected with selection effects. In general, optical afterglows (crucial for redshift determination) of type I bursts are fainter than ones of type II bursts, and therefore are harder to detect at high redshift (e.g. Kann et al. 2011). Secondly, type I bursts are generated by a merger of compact components in old binary systems, which could not occur at a high redshift due to a long evolution of the

**Table 2.** Observed parameters of investigated subsamples.

Subsample	N	$z$ [min]	$z$ [median]	$z$ [max]	$E_{\text{iso}}$ [median] $10^{51}$ erg	$E_{\text{p},i}$ [median] keV	$T_{90,i}$ [median] s
I	45	0.0097	0.46	3.05	0.68	706	0.27
I + EE	11	0.125	0.41	1.72	3.2	909	0.58
I w/o EE	34	0.0097	0.51	3.05	0.57	662	0.25
II	275	0.0085	1.60	8.10	100	446	14.5
II + SN	40	0.0085	0.55	1.06	8.98	134	23.8
II w/o SN	235	0.12	1.90	8.10	122	512	13.6
II $z_1$	55	0.0085	0.53	0.76	9.15	218	24.6
II $z_2$	55	0.78	1.00	1.31	70.4	372	13.1
II $z_3$	55	1.32	1.60	2.01	130	540	14.5
II $z_4$	55	2.01	2.30	2.82	230	694	10.0
II $z_5$	55	2.82	3.65	8.10	176	575	11.2

system towards merging (e.g. Guetta & Piran 2005). In our sample, the most distant type I burst is GRB 081024B with  $z = 3.05$ , the most distant type II burst is GRB 090423 with  $z = 8.1$  (both values are not spectroscopic).

Type I bursts with an extended emission (I+EE) do not differ from the regular ones in terms of redshift distribution, having similar  $z$  median values. It reveals negligible selection effects of the extended emission detection: if the extended emission is a weak component, the redshift distribution for I+EE bursts is expected to be shifted towards low redshift values. It indicates the same progenitor type for both subsamples (e.g. no difference in a merging delay), but the presence of two separate subclasses of type I bursts.

Type II bursts associated with Ic supernova (II+SN) demonstrate the opposite behavior. The redshift distribution for II+SN bursts is significantly shifted to low values comparing with regular type II bursts (median values are  $z = 0.55$  and  $z = 1.90$ , correspondingly). The difference is obviously connected with strong selection effects: supernova signatures (photometric, and spectroscopic especially) are very difficult to reveal at large distances ( $z \gtrsim 1$ ) with present optical telescopes. It is confirmed by the fact that the closest type II bursts ( $z \lesssim 0.3$ ) are mostly accompanied by supernovae (see Fig. 1), which may indicate that all type II GRBs are accompanied by Ic supernovae. The biased redshift distribution for II+SN bursts leads to significant biases in other parameter distributions (Sections 2.2.2, 2.2.3, 2.2.4).

### 2.2.2 Duration, $T_{90,i}$

The dependence of  $T_{90,i}$  on redshift for both GRB types is presented at the left graphs of Fig. 1.

Type I bursts are 50 times shorter than type II ones: the median values are  $T_{90,i} = 0.27$  s and  $T_{90,i} = 14.5$  s, correspondingly. Four type I bursts are longer 1 s and four type II bursts are shorter 1 s, confirming high overlap of a duration distribution and its weak reliability as a blind classification method.

Our sample contains four ultralong bursts with  $T_{90,i} > 1000$  s. We find no peculiarities of these bursts except the duration. The nature of ultralong GRBs and their possible separation into a different burst class are still debatable (e.g. Gendre et al. 2019).

The lack of bursts with a duration in the interval (200,

2000) s could be connected (at least, partially) with selection effects. Long GRBs ( $T_{90} > 200$  s) are difficult to register due to background variations and due to source occultation by the Earth in experiments on low orbits (Fermi, Swift) or due to telemetry limitations (Konus-Wind). Therefore, the  $T_{90,i}$  distribution becomes asymmetric for type II bursts, having sharper “long” edge and well fitted by a skewed gaussian (see Section 4, equation (4) and Fig. 5). In addition, the rest frame duration,  $T_{90,i} = \frac{T_{90}}{1+z}$  decreases with redshift (shown by dotted lines at left graphs in Fig. 1). As a consequence, the duration of long and distant bursts is underestimated most probably due to selection effects (see the  $z_5$  subsample of type II bursts at Fig. 1).

There is also a lack of relatively short ( $T_{90,i} < 4$  s) type II bursts at low redshift ( $z < 0.4$ ,  $z_1$  subsample). These bursts are also fainter ( $E_{\text{iso}} < 10^{52}$  erg) and softer ( $E_{\text{p},i} < 200$  keV) comparing with more distant bursts (see Fig. 1). In Norris et al. (2005) was shown, that long bursts with wide pulses are also fainter and softer. Therefore, the lack is possibly connected with selection effects.

All discussed selection effects can lead to a negative  $z - T_{90,i}$  correlation for type II bursts. We check the possible correlation using the Spearman rank-order correlation coefficient ( $\rho$ ) and the associated null-hypothesis (chance) probability, or  $P_\rho$  value. The null hypothesis is that no correlation exists; therefore, a small  $P_\rho$  value indicates a significant correlation. We apply this method to analyze other correlations through the paper. As expected, we do not detect the correlation for type I bursts ( $\rho = -0.006$ ,  $P_\rho = 0.97$ ), but find the negative correlation for type II bursts ( $\rho = -0.21$ ,  $P_\rho = 5.2 \times 10^{-4}$ ). The result is also confirmed by a slight decreasing of median  $T_{90,i}$  values with increasing of  $z$  for  $z_1 - z_5$  type II bursts subsamples (see Table 2).

I+EE bursts are longer than regular type I bursts: median values are  $T_{90,i} = 0.58$  s and  $T_{90,i} = 0.25$  s, correspondingly. Most (four of five) type I bursts, having  $T_{90,i} > 1$  s, are from type I+EE subsample. It possibly confirms the definition of I+EE bursts as a separate subclass of type I bursts. As one of the possible scenarios, a merging of neutron stars under some circumstances (affecting also prompt emission properties) could result in the forming of magnetar, responsible for an extended emission component (e.g. Metzger et al. 2008).

As was shown earlier, a subsample of II+SN bursts is

affected by strong selection effects. II+SN bursts, representing mostly the closest  $z_1$  subsample, are longer than regular type II bursts, as a consequence: median values are  $T_{90,i} = 23.8$  s and  $T_{90,i} = 13.6$  s, correspondingly. Nevertheless, they cover a whole range of  $T_{90,i}$  values for type II bursts, confirming the suggestion, that they do not differ from regular type II bursts, meaning all type II bursts are accompanied by SN Ic.

### 2.2.3 Total isotropic equivalent energy release, $E_{iso}$

Type I bursts are 100 times fainter than type II bursts: median values are  $E_{iso} = 6.8 \times 10^{50}$  erg and  $E_{iso} = 1.0 \times 10^{53}$  erg, correspondingly.

The dependence of  $E_{iso}$  on redshift for both GRB types is presented in the middle graphs of Fig. 1. The dependence is highly affected by selection effects for both GRB types. Dotted curves at Fig. 1 show the  $E_{iso}(z)$  dependence for a fixed fluence  $F$ , representing a sensitivity of a gamma-ray detector to triggering a burst. As a consequence, we can detect weak bursts only at low redshift: the bottom-right side of the  $z - E_{iso}$  diagram is empty due to selection effects.

One can see also at Fig. 1 the increasing of the number of bright bursts with increasing of a redshift for both GRB types. It can be explained by the non-flat luminosity function for GRBs: bright bursts are more rare, than weak ones.

All these selection effects lead to a significant positive  $z - E_{iso}$  correlation for both GRB types:  $\rho = 0.69$  and  $P_\rho = 1.6 \times 10^{-7}$  for type I bursts,  $\rho = 0.46$  and  $P_\rho = 1.9 \times 10^{-15}$  for type II bursts. It is also supported by median values of  $z_1 - z_5$  subsamples (see Table 2).

I+EE bursts are brighter than regular ones in terms of median values ( $E_{iso} = 3.2 \times 10^{51}$  erg and  $E_{iso} = 0.57 \times 10^{51}$  erg, correspondingly), but they are not concentrated to the top of the  $E_{iso}$  distribution and cover a whole range of observable  $E_{iso}$  values of type I bursts. Therefore, we cannot draw a definitive conclusion about their difference in  $E_{iso}$  from regular type I bursts. It could be accidental.

II+SN bursts are significantly fainter than regular type II bursts in terms of median values:  $E_{iso} = 9.0 \times 10^{51}$  erg and  $E_{iso} = 1.22 \times 10^{53}$  erg, correspondingly. It could be explained by the selection effects, described above (Section 2.2.1). The covering of the whole range of  $E_{iso}$  distribution by them supports the suggestion.

### 2.2.4 The position of the extremum (maximum) in $vF_v$ spectrum, $E_{p,i}$

The dependence of  $E_{p,i}$  on redshift for both GRB types is presented in the right graphs of Fig. 1.

Type I bursts are 1.5 times harder ( $E_{p,i} = 706$  keV vs  $E_{p,i} = 446$  keV), than type II bursts. The behavior of all subsamples on  $z - E_{p,i}$  diagram is analogous to their behavior on  $z - E_{iso}$  diagram. It could be explained by the presence of the  $E_{p,i} - E_{iso}$  correlation. We find significant positive  $z - E_{p,i}$  correlation for type II bursts ( $\rho = 0.40$  and  $P_\rho = 3.7 \times 10^{-12}$ ) and the weak positive correlation for type I bursts ( $\rho = 0.52$  and  $P_\rho = 2.4 \times 10^{-4}$ ).

A possible selection effect at the  $z - E_{p,i}$  diagram is

connected with a limited working energy range of gamma-ray detectors. If  $E_{p,i}$  is placed outside the range, it could not be determined. A typical value of a lower energy range bound of modern detectors is  $\sim 10$  keV. The corresponding trajectory  $E_{p,i} = E_p(1 + z)$  is shown by the dotted curve at top right graph in Fig. 1. At high redshift ( $z = 5$ ) it becomes  $E_{p,i} = 60$  keV, while the minimal observed value is  $\sim 5$  times larger (type II bursts sample). It means the possible selection effect of the detector lower energy range bound is minimal.

The situation with the upper energy bound is more complicated, because the  $E_{p,i}$  determination depends also on count statistics, which is low at high energies due to the hard intrinsic GRB energy spectrum and due to decreasing of the effective area of detectors. The influence of this effect needs detailed investigation, which is beyond the scope of the paper. Here, we suppose this effect to be small and consider the evolution of  $E_{p,i}$  with redshift to be real, suggesting the connection of observable  $z - E_{p,i}$  correlation with  $z - E_{iso}$  and  $E_{p,i} - E_{iso}$  correlations. To confirm that, we investigated a possible evolution of  $E_{p,i} - E_{iso}$  correlation with redshift for type II bursts (see Section 3.4).

## 3 THE $E_{p,i} - E_{iso}$ CORRELATION

### 3.1 Fitting the correlation

The  $E_{p,i} - E_{iso}$  diagram constructed for different subsamples (regular type I bursts, I+EE bursts, regular type II bursts, II+SN bursts) is presented at Fig. 2.

To confirm the existence of correlations we calculate the Spearman rank-order correlation coefficients ( $\rho$ ) and the associated null-hypothesis (chance) probabilities or  $P_\rho$  values (Table 3). For whole type I and type II samples correlation parameters are  $\rho = 0.80$  ( $P_\rho = 4.6 \times 10^{-11}$ ) and  $\rho = 0.77$  ( $P_\rho < 1 \times 10^{-50}$ ), correspondingly, indicating a strong correlation for both samples. The correlation for type I bursts was confirmed for the first time with such high probability level. A strong correlation is also found for II+SN subsample ( $\rho = 0.73$  and  $P_\rho = 8.8 \times 10^{-8}$ ), while the correlation of I+EE subsample is not highly significant ( $\rho = 0.83$  and  $P_\rho = 1.7 \times 10^{-3}$ ), due to the small number of events.

The correlation is characterized by the “intrinsic” scatter for all subsamples: the observed scatter of the correlation is sufficiently larger than the other one connected with statistical errors only (see e.g. Heussaff et al. 2013; Tsvetkova et al. 2017). The intrinsic scatter dominates on the statistical one for the brightest bursts (see e.g. type II bursts with  $E_{iso} > 10^{54}$  erg at Fig. 2). Its presence is confirmed by the  $\chi^2_{\text{red}} \gg 1$ . The nature of the intrinsic scatter is unknown, it could be connected with underestimated systematics (e.g. obtained during spectral fitting and determining of  $E_p$ ) or with GRB progenitor features. It makes GRBs not standard candles, even when using the  $E_{p,i} - E_{iso}$  correlation for “standardizing” them.

To fit the correlation (equation (1)), we transform  $E_{p,i}$  and  $E_{iso}$  values to  $x = \lg\left(\frac{E_{iso}}{10^{51} \text{ erg}}\right)$  and  $y = \lg\left(\frac{E_{p,i}}{100 \text{ keV}}\right)$  and perform linear model fitting ( $y = ax + b$ ) with considering of statistical errors for both  $x$  and  $y$  values using several

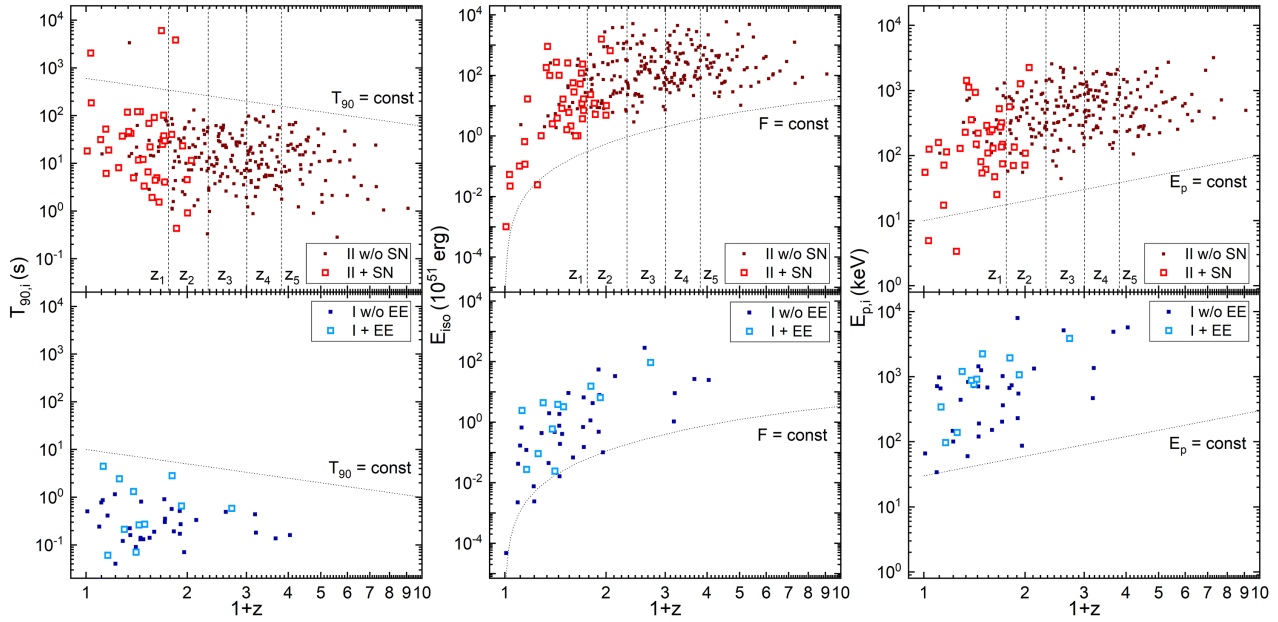


**Figure 1.** The dependence of  $T_{90,i}$  (left),  $E_{\text{iso}}$  (middle) and  $E_{p,i}$  (right) parameters on redshift, for regular type I bursts (blue dots) and type I bursts with extended emission (cyan squares) at bottom figures, regular type II bursts (dark red dots) and type II bursts associated with Ic supernova (red squares) at top figures. Vertical dashed lines show bounds of  $z_1 - z_5$  subsamples of type II bursts. Dotted lines represent the dependence of intrinsic rest frame parameters on redshift for parameters fixed in the observer frame.

**Table 3.** The  $E_{p,i} - E_{\text{iso}}$  correlation fit parameters for investigated subsamples.

Subsample	N	$\rho$	$P_\rho$	$a_{\text{York}}$	$b_{\text{York}}$	$a_{\text{Deming}}$	$b_{\text{Deming}}$	$a$	$b$
I	45	0.80	$4.6 \times 10^{-11}$	$0.45 \pm 0.03$	$0.86 \pm 0.04$	$0.37 \pm 0.04$	$0.81 \pm 0.05$	$0.41 \pm 0.05$	$0.83 \pm 0.06$
I + EE	11	0.83	$1.7 \times 10^{-3}$	$0.40 \pm 0.07$	$0.80 \pm 0.05$	$0.36 \pm 0.10$	$0.83 \pm 0.10$	$0.38 \pm 0.12$	$0.82 \pm 0.11$
I w/o EE	34	0.81	$7.1 \times 10^{-9}$	$0.45 \pm 0.03$	$0.88 \pm 0.05$	$0.37 \pm 0.04$	$0.80 \pm 0.06$	$0.41 \pm 0.05$	$0.84 \pm 0.08$
II	275	0.77	$< 1 \times 10^{-50}$	$0.47 \pm 0.02$	$-0.36 \pm 0.04$	$0.38 \pm 0.02$	$-0.12 \pm 0.04$	$0.43 \pm 0.03$	$-0.24 \pm 0.06$
II + SN	40	0.73	$8.8 \times 10^{-8}$	$0.57 \pm 0.04$	$-0.58 \pm 0.10$	$0.34 \pm 0.05$	$-0.13 \pm 0.08$	$0.46 \pm 0.07$	$-0.36 \pm 0.13$
II w/o SN	235	0.73	$9.0 \times 10^{-40}$	$0.41 \pm 0.02$	$-0.23 \pm 0.05$	$0.39 \pm 0.03$	$-0.12 \pm 0.06$	$0.40 \pm 0.03$	$-0.18 \pm 0.07$
II $z_1$	55	0.69	$6.2 \times 10^{-9}$	$0.58 \pm 0.04$	$-0.56 \pm 0.09$	$0.33 \pm 0.05$	$-0.06 \pm 0.07$	$0.45 \pm 0.06$	$-0.31 \pm 0.11$
II $z_2$	55	0.76	$1.4 \times 10^{-11}$	$0.42 \pm 0.03$	$-0.29 \pm 0.08$	$0.37 \pm 0.05$	$-0.14 \pm 0.09$	$0.39 \pm 0.05$	$-0.22 \pm 0.12$
II $z_3$	55	0.67	$1.7 \times 10^{-8}$	$0.44 \pm 0.04$	$-0.31 \pm 0.13$	$0.48 \pm 0.07$	$-0.32 \pm 0.16$	$0.46 \pm 0.09$	$-0.32 \pm 0.21$
II $z_4$	55	0.73	$2.1 \times 10^{-10}$	$0.34 \pm 0.05$	$-0.03 \pm 0.13$	$0.41 \pm 0.05$	$-0.19 \pm 0.13$	$0.38 \pm 0.07$	$-0.11 \pm 0.18$
II $z_5$	55	0.69	$4.3 \times 10^{-9}$	$0.40 \pm 0.04$	$-0.12 \pm 0.11$	$0.46 \pm 0.06$	$-0.28 \pm 0.14$	$0.43 \pm 0.07$	$-0.20 \pm 0.18$

different methods. Fitting the correlation is appeared to be tricky because of the intrinsic scatter presence.

$$\lg \left( \frac{E_{p,i}}{100 \text{ keV}} \right) = a \lg \left( \frac{E_{\text{iso}}}{10^{51} \text{ erg}} \right) + b. \quad (1)$$

Firstly, we use the  $\chi^2 = \sum_{i=1}^N \frac{(y_i - ax_i - b)^2}{a^2 \sigma_{x_i}^2 + \sigma_{y_i}^2 + \sigma_{\text{int}}^2}$  minimization method, which introduces additional intrinsic scatter component  $\sigma_{\text{int}}$  in the weights calculation (Tremaine et al. 2002)). The method was used for the  $E_{p,i} - E_{\text{iso}}$  correlation fitting in Tsvetkova et al. (2017). The intrinsic scatter  $\sigma_{\text{int}}$  is estimated from the  $\chi^2_{\text{red}} = 1$  condition.

Introducing  $\sigma_{\text{int}}$  in the fitting changes results significantly comparing with  $\sigma_{\text{int}} = 0$  situation. We found the fit results with  $\sigma_{\text{int}}$  to be similar with the fitting without considering errors at all. Indeed, introducing  $\sigma_{\text{int}}$  equalizes the fit weights, it leads to significant weight decrease for bursts

with high S/N. Despite the fact, that both  $\sigma_x$  and  $\sigma_y$  errors are included in the approximation, the method measures the deviation of the data against the model in direction parallel to the  $y$  axis. As a consequence, fit parameters change dramatically with  $x \rightarrow y$  and  $y \rightarrow x$  replacing (e.g. for the whole type II sample the power-law index changes from  $a = 0.35 \pm 0.02$  to  $a = 0.55 \pm 0.03$ ). Therefore, we do not use this method to fit the correlation.

We found York (York et al. 2004) and Deming (Deming 2011) approximation methods to be reliable, considering both  $\sigma_x$  and  $\sigma_y$  errors, not sensitive to  $x \rightarrow y$  and  $y \rightarrow x$  replacing. We used them both, because they give slightly different parameter values. As a final fit, used for further analysis, we suggest mean values of the fit parameters,  $a = \frac{1}{2}(a_{\text{York}} + a_{\text{Deming}})$  and  $b = \frac{1}{2}(b_{\text{York}} + b_{\text{Deming}})$ .

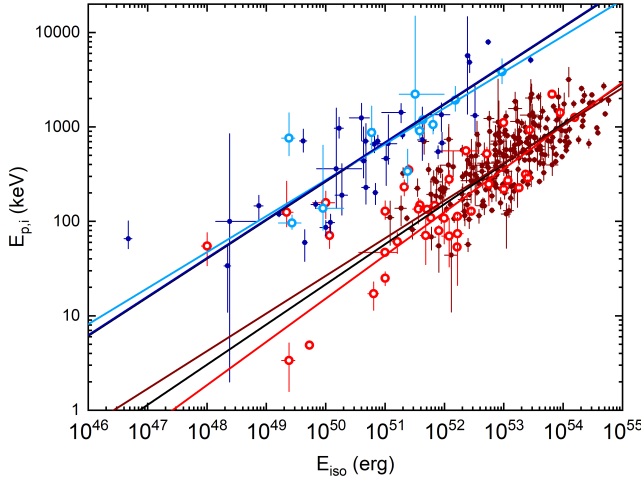


**Figure 2.** The  $E_{p,i} - E_{iso}$  correlation for subsamples of regular type I bursts (blue dots), type I bursts with an extended emission (cyan circles), regular type II bursts (dark red dots) and type II bursts with an associated supernova (red circles). Corresponding fits are shown by the colored lines (black lines represent fits of the whole type I and type II samples). Uncertainties for  $E_{iso}$  and  $E_{p,i}$  are presented at the  $1\sigma$  significance level.

Corresponding parameter errors are calculated as  $\sigma_a = \sqrt{\sigma_{a_{York}}^2 + \sigma_{a_{Deming}}^2}$  and  $\sigma_b = \sqrt{\sigma_{b_{York}}^2 + \sigma_{b_{Deming}}^2}$ .

### 3.2 The approximation results

The approximation results are summarized in Table 3 and shown at Fig. 2. Power-law indexes ( $a$ ) of the correlation are found to be the same (within  $1\sigma$ ) for all investigated subsamples,  $a \approx 0.4$ , while  $b$  values differ significantly: the correlation for type I bursts is shifted up against the one for type II bursts. These features could be used in a blind GRB classification (see Section 4). The fact of similar power-law index value for both GRB types confirms results obtained in Zhang et al. (2018b).

Type I bursts with an extended emission and regular type I bursts follow the same correlation, possibly indicating the same progenitors and emission mechanism. We obtain similar results for type II bursts associated with Ic supernovae and for regular type II bursts.

One of possible explanations of the  $E_{p,i} - E_{iso}$  correlation is connected with viewing angle effects. In the model, the value of the power-law index depends on the structure of the ejecta: e.g.  $E_{p,i} \sim E_{iso}^{1/3}$  if it is a cone relativistic jet emission, and  $E_{p,i} \sim E_{iso}^{1/4}$  if it is a spherical relativistic emission (e.g. Eichler & Levinson 2004; Levinson & Eichler 2005; Pozanenko et al. 2018). The derived value of the power-law index,  $a \approx 0.4$  is close to the cone relativistic jet emission. The same power-law index for both GRB types can indicate the same structure of the jet for both GRB types.

In the model of connection of  $E_{p,i} - E_{iso}$  correlation with viewing angle effects, bursts observed close to axis are brighter and harder, placed at top-right in the  $E_{p,i} - E_{iso}$  plane, while the bursts seen off-axis are placed in bottom-left of the plane. GRB 170817A, associated with gravitational

wave event GW 170817, is the principal candidate for an off-axis burst, being the faintest GRB with  $E_{iso} < 10^{47}$  erg (Fig. 2). Several signs of observing this burst at a large angle to the jet axis were actually discovered, supporting the viewing angle model. One can mention the absence of the X-ray afterglow at early stages and a powerful kilonova component in optical range, comparing with a standard optical a power-law like afterglow emission (e.g. Pozanenko et al. 2018).

### 3.3 Outliers of the correlation for type II bursts

Three type II bursts are found to be placed outside a  $3\sigma_{cor}$  correlation region: GRB 980425B, GRB 031203A, and GRB 171205A. We consider them as outliers of the correlation. The  $\sigma_{cor}$  corresponds to the “real” scatter of the correlation, representing both statistical and intrinsic scatter and estimated as empirical standard deviation of the points from the correlation:  $\sigma_{cor} = \sqrt{\frac{\sum_{i=1}^n (y_i - \bar{y}_i)^2}{n-1}}$ , where  $\bar{y}_i = ax_i + b$ . We also fit the  $E_{p,i} - E_{iso}$  correlation for type II bursts sample and its subsamples with outliers excluded and find the parameters of the correlation to be similar (within  $1\sigma$ ) with ones obtained for subsamples with outliers included.

All three bursts are known outliers and are placed above the  $E_{p,i} - E_{iso}$  correlation. Their peculiarity is still a subject of debate (e.g. Ghisellini et al. 2006; Daigne & Mochkovitch 2007; Nava et al. 2012; D’Elia et al. 2018), with the following possible interpretations: 1) a normal (intrinsically bright) gamma-ray burst seen off-axis, 2) the burst with different emission mechanism, or 3) an intrinsically weak gamma-ray burst seen on-axis through a scattering screen. These bursts are among the faintest over the investigated type II sample, having  $E_{iso} \leq 10^{50}$  erg. Excluding them, there are only two type II bursts with  $E_{iso} \leq 10^{50}$  erg, both are X-ray flashes (XRFs), GRB 020903 and GRB 060218. It leads us to several questions, which should be answered in future works. 1) How is the sample of the faintest ( $E_{iso} < 10^{50}$  erg) and closest as a consequence ( $z \leq 0.1$ ) bursts biased? 2) Do the closest bursts ( $z \leq 0.1$ ) belong to the different progenitor population? 3) Do the faintest bursts have a different emission mechanism?

To conclude, the nature of the outliers and the behavior of the correlation for the faintest type II bursts ( $E_{iso} < 10^{50}$  erg) remain unresolved. Increasing the sample of the faintest bursts could shed light on a problem.

### 3.4 The evolution of the $E_{p,i} - E_{iso}$ correlation with redshift for type II bursts

The extensive sample of type II bursts (275 events) allows us to investigate the evolution of the  $E_{p,i} - E_{iso}$  correlation. We formed five subsamples ( $z_1 - z_5$ ).

The  $E_{p,i} - E_{iso}$  correlation for  $z_1 - z_5$  subsamples and corresponding power-law fits are presented in Fig. 3 and summarized in Table 3. We do not detect the significant evolution of the correlation with the redshift. All subsamples have similar (within  $1\sigma$ ) power-law index,  $a \approx 0.4$ . It indicates, that the correlation is not connected with selection effects and confirms negligible selection effects in measuring of  $E_{p,i}$ , discussed in Section 2.2.4.

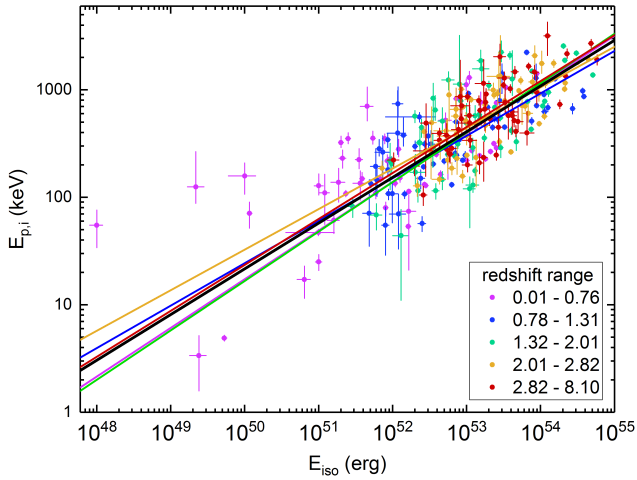


**Figure 3.** The  $E_{\text{p},i} - E_{\text{iso}}$  correlation for five subsamples of type II bursts (magenta is for  $z_1$  subsample, blue –  $z_2$ , green –  $z_3$ , orange –  $z_4$ , red –  $z_5$ ). Redshift intervals for the subsamples are shown in the legend. Uncertainties for  $E_{\text{iso}}$  and  $E_{\text{p},i}$  are presented at the  $1\sigma$  significance level. Corresponding fits for the whole sample (black line) and for the subsamples (colored lines) are shown.

#### 4 NEW CLASSIFICATION SCHEME

The motivation of introducing new classification scheme is connected with phenomenological differences between type I and type II bursts, discussed in the paper.

##### 4.1 Classification parameters $EH$ and $EHD$

The  $E_{\text{p},i} - E_{\text{iso}}$  correlation for type I bursts sample is found to be well-distinguished from the one constructed for type II bursts and has a similar power-law index value,  $E_{\text{p},i} \sim E_{\text{iso}}^{0.4}$  (Fig. 2). Therefore, it can be used for a blind classification of GRBs: the distribution of burst deviations from the power-law dependence  $E_{\text{p},i} \sim E_{\text{iso}}^{0.4}$  should be bimodal. The deviation could be measured by the parameter  $EH$  (“Energy-Hardness”) – the combination of  $E_{\text{p},i}$  and  $E_{\text{iso}}$  parameters (Equation 2). Type I bursts are harder (higher value of  $E_{\text{p},i}$ ) and fainter (lower value of  $E_{\text{iso}}$ ) than type II ones in general, therefore they are characterized by a higher value of  $EH$  parameter. The  $E_{\text{p},i}$  value alone is analogous to the commonly used hardness ratio (HR) parameter.

$$EH = \frac{(E_{\text{p},i}/100 \text{ keV})}{(E_{\text{iso}}/10^{51} \text{ erg})^{0.4}}. \quad (2)$$

The second proposed classification parameter follows the bimodal nature of duration distribution: type I bursts are shorter than type II ones. Although  $T_{90,i}$  value is highly affected by selection effects and some intrinsic properties, it can be a good additional classification indicator.

The  $T_{90,i} - EH$  diagram is presented at Figure 4. Type I bursts are placed at the top left on the diagram being short hard and faint, comparing with type II bursts. The separation of the clusters is not satisfactory, when using only  $T_{90,i}$  (separation, parallel to y-axis) or  $EH$  (separation, parallel to x-axis) parameters. Good separation is reached

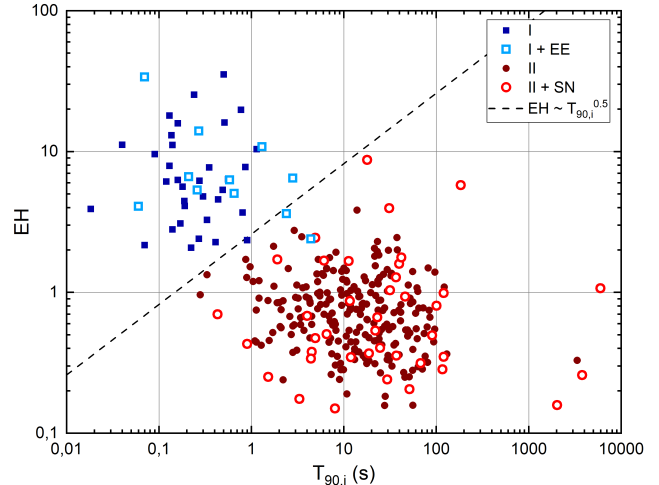


**Figure 4.** The  $T_{90,i} - EH$  diagram for I+EE bursts (cyan open squares), regular type I bursts (blue squares), II+SN bursts (red open circles) and type II (dark red circles) bursts. The power-law dependence with index of 0.5 (dashed line) represents the clusters separation.

with the dashed line,  $EH \sim T_{90,i}^{0.5}$ . Therefore, we can modify the  $EH$  parameter by including the duration  $T_{90,i}$  into a consideration and obtain the second classification parameter,  $EHD$  (“Energy-Hardness-Duration”, equation 3). Purely phenomenological,  $EHD$  parameter results in the best separation of type I bursts from type II ones.

$$EHD = \frac{EH}{(T_{90,i}/1 \text{ s})^{0.5}} = \frac{(E_{\text{p},i}/100 \text{ keV})}{(E_{\text{iso}}/10^{51} \text{ erg})^{0.4} (T_{90,i}/1 \text{ s})^{0.5}}. \quad (3)$$

Dividing the  $EH$  parameter by  $T_{90,i}^{0.5}$  for type II bursts, having  $T_{90,i} \gg 1$  s, leads to lower values of  $EHD$  for them and better separation from type I bursts.

The investigation of a physical meaning of EH and EHD parameters is beyond the scope of the paper, but they might be due to principal differences of progenitors: e.g., central engine of type I bursts could generate harder emission with higher Lorentz factor, but operate for shorter time, comparing with type II bursts.

##### 4.2 Testing the reliability of different classification schemes

To investigate the reliability of the GRB classification, based on observational parameters  $EH$ ,  $EHD$  and  $T_{90,i}$ , we analyze corresponding parameter distributions, presented at Fig. 5.

###### 4.2.1 Fitting the distributions

We perform a blind approximation of distributions. It suggests the approximation of the total (type I + type II samples) parameter distribution by sum of two functions, representing two types of bursts.

The duration ( $T_{90,i}$ ) distribution is fitted in a logarithmic scale by sum of gaussian and skewed gaussian (equa-

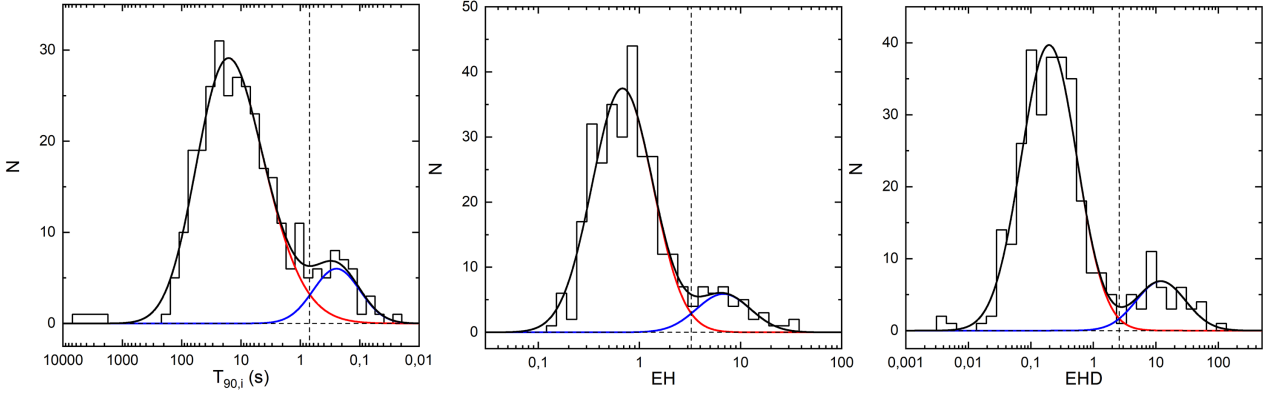


**Figure 5.** The distributions of the  $T_{90,i}$  (left),  $EH$  (middle), and  $EHD$  (right) parameters for whole samples of type I and type II bursts. Blue (red) curves represent distribution fits for type I (type II) burst modes, while black curves show total fit. The intersection points of type I and type II modes fits are shown by vertical dashed lines.

**Table 4.** Parameters of investigated distributions.

Distr.	GRB	A	$x_0$	$\omega$	$\alpha$
$T_{90,i}$	I	$5.9 \pm 0.7$	$-0.61 \pm 0.05$	$0.39 \pm 0.05$	0
	II	$42.1 \pm 0.8$	$1.64 \pm 0.01$	$0.79 \pm 0.02$	-1.5
$EH$	I	$4.0 \pm 0.5$	$0.83 \pm 0.03$	$0.27 \pm 0.04$	0
	II	$28.3 \pm 0.5$	$-0.16 \pm 0.01$	$0.30 \pm 0.01$	0
$EHD$	I	$6.8 \pm 0.6$	$1.08 \pm 0.04$	$0.40 \pm 0.04$	0
	II	$44.3 \pm 0.6$	$-0.71 \pm 0.01$	$0.45 \pm 0.01$	0

tion 4), representing type I and type II bursts, correspondingly. Using skewed gaussian instead of regular gauss function for type II burst mode is connected with deformation of the distribution at the left side (large  $T_{90,i}$  values) probably due to several selection effects, discussed earlier (see Section 2.2.2). We fix the skew parameter in the fitting,  $\alpha = -1.5$ . The equation 4 with  $\alpha = 0$  corresponds to the regular gaussian. The possibility of using skewed gaussian to fit duration distribution is also discussed e.g. in Tarnopolski (2016). Other distributions ( $EH$  and  $EHD$ ) are fitted by sum of two regular gaussians ( $\alpha = 0$ ) in a logarithmic scale. Fit results are summarized in Table 4 and shown in Fig. 5.

$$N = \frac{A}{\sqrt{2\pi\omega^2}} \exp\left(-\frac{(x-x_0)^2}{2\omega^2}\right) \left[1 + \text{erf}\left(\frac{\alpha(x-x_0)}{\sqrt{2\omega^2}}\right)\right]. \quad (4)$$

#### 4.2.2 Testing the different classification methods reliability

Traditional GRB blind classification method, based on the duration distribution in the observer frame, uses the position of the distribution minimum, observed at  $T_{90} \sim 2$  s (e.g. Kouveliotou et al. 1993). In the rest frame the position of the minimum is shifted towards short durations ( $T_{90,i}$  distribution). It is close to the intersection point (dashed vertical line at Fig. 5, left) of individual modes of two burst types (blue and red dashed curves at Fig. 5, left). The intersection point is placed at  $T_{90,i} = 0.7$  s in our sample. We use the intersection point as the separation line in a blind classification for all investigated distributions.

As seen at Fig. 5, modes representing type I and type II samples in the duration distribution, are highly overlapped.

The intersection point is placed at a half of the height of type I distribution, the contribution of type II mode is significant down to  $T_{90,i} \sim 0.2$  s. We can estimate the distributions overlap numerically by calculating the portion of the type I (type II) bursts with  $T_{90,i}$  larger (smaller) than the intersection value (0.7 s), using the corresponding model functions derived in the blind fitting procedure (Table 4). While the most of type II bursts (97.7 %) are within the interval  $T_{90,i} > 0.7$  s, more than 12 % of type I bursts are outside the  $T_{90,i} < 0.7$  s region. These values correspond to the expected portion of falsely classified bursts. It makes the reliability of  $T_{90,i}$  based classification low.

To check the reliability of the  $T_{90,i}$  based classification method, we perform a blind classification of bursts from our sample. 9 type I bursts (20 % of the sample) and 3 type II bursts (1 % of the sample) are classified falsely, having  $T_{90,i}$  larger or smaller than 0.7 s, correspondingly (Table 5). The portion of falsely classified bursts roughly follows the expected value, based on the overlap of the distribution. I+EE bursts are the most significant outliers in the duration distribution with GRB 060614A being the “leader” ( $T_{90,i} = 4.4$  s).

We perform the same analysis for  $EH$  and  $EHD$  distributions. The results are summarized in Table 5. The  $EH$  distribution gives better results, comparing with the  $T_{90,i}$  one. The separation point is placed at  $EH = 3.3$ , which gives comparable overlapping: 12 % of type I and 1.1 % of type II bursts are placed beyond the separation point. 9 type I bursts and 4 type II bursts are falsely classified using  $EH$ -based blind classification scheme. The most significant outliers in type II sample are known outliers of the  $E_{p,i} - E_{iso}$  correlation (GRB 980425B, GRB 031203 and GRB 171205A, see Section 3.3). Among 9 type I bursts, falsely classified, only GRB 060614A represents the subsample of I+EE bursts.

The best results are obtained for  $EHD$  distribution. The separation point is placed at  $EHD = 2.6$  with almost negligible overlapping: 6.5 % of type I and 0.6 % of type II bursts are placed beyond the separation point. Only three type I bursts (GRB 050724A, GRB 060614A and GRB 131004A) are falsely classified using  $EHD$ -based blind classification scheme. All type II bursts are classified correctly.

GRB 050724A is classified correctly in  $EH$ -based

**Table 5.** The reliability of different blind classification schemes.

Distribution	Type I <sup>a</sup>	Type II <sup>a</sup>	Separation <sup>b</sup>
$T_{90,i}$	12.4% (9)	2.3% (3)	0.7 s
$EH$	12.1% (9)	1.1% (4)	3.3
$EHD$	6.5% (3)	0.6% (0)	2.6

<sup>a</sup> the expected portion of bursts beyond the separation line with the real number of false blind classifications for the sample in brackets.

<sup>b</sup> the position of the separation line.

scheme, being outlier in duration-based scheme. It is not significant outlier in  $EHD$ -based scheme, having  $EHD = 2.33$  with  $EHD = 2.6$  used for classification. It may indicate, that its false classification could be accidental. Indeed, the  $E_{p,i}$  parameter is determined for the burst with large errors:  $E_{p,i} = 138^{+503}_{-57}$  keV (Table A). Changing  $E_{p,i}$  to 200 keV results in  $EHD = 3.4$ , making the burst to be from type I population.

Falsely classified in all three classification schemes GRB 060614A is a known outlier, demonstrating observational features of type II bursts, except the absence of supernova component (e.g. Gehrels et al. 2006). Nevertheless, it probably belongs to I+EE population, confirmed by a marginal detection of a kilonova emission, characteristics of type I bursts (Yang et al. 2015). The possible solution of its peculiarity is discussed in the Section 4.3.

GRB 131004A is also classified falsely in all three classification schemes, but the discrepancy is not highly significant. The  $E_{p,i}$  value was not measured precisely ( $E_{p,i} = 202 \pm 51$  keV), so the false classification could be accidental. Therefore, we can not exclude the burst as the type I one.

As was mentioned before, GRB 170817A (the first gamma-ray burst associated with gravitational waves) is placed in the middle of the overlap region of hardness ratio and duration distributions (e.g. Goldstein et al. 2017), confusing its blind classification. But the burst is clearly classified as the type I burst in our both,  $EH$  and  $EHD$  classification methods, emphasizing their high reliability.

To conclude,  $EHD$ -based classification method is the most reliable one for a blind classification of GRBs. The values of  $EH$  and  $EHD$  parameters along with the GRB type based on the corresponding blind classification are presented in Table A for all bursts.

### 4.3 Using $EHD$ -based classification scheme for GRBs with no redshift

Although  $EHD$ -based classification gives the most reliable results, it is based on redshift and  $E_p$  values, which are obtained for a very small portion (< 10 %) of observed gamma-ray bursts. Let us investigate the dependence of  $EH$  and  $EHD$  parameters on redshift.

The trajectory of GRB 060614A on  $T_{90,i} - EH$  diagram, as a function of redshift in the interval  $z = (0.01, 10)$ , is shown by a black curve in Fig. 6. The measured redshift for the burst ( $z = 0.1254$ ) corresponds to the cyan square symbol and characterizes the burst as the type II one. The trajectory crosses the classification line ( $EHD = 2.6$ , dashed line at Fig. 6) at  $z \approx 0.03$ . So, the burst could be classified as the type I one, if  $z < 0.03$ .

It is possible, that redshift of GRB 060614A is determined wrong. It is measured only for a supposed host galaxy, placed  $0.5''$  from the burst optical counterpart. The estimated chance probability of the observed offset between the GRB and the galaxy ranges from  $P = 2 \times 10^{-5}$  in Gehrels et al. (2006) to  $P \approx 0.01$  in Cobb et al. (2006). So, the association of the burst with the galaxy could be accidental, and the burst could be placed in outskirts of other nearby galaxy with  $z < 0.03$ . This suggestion is also supported by unusually high mass of ejecta of detected kilonova for the event, estimated for  $z = 0.125$  (Jin et al. 2016; Tanaka 2016). Placing the burst at lower redshift eliminates the peculiarity.

We investigated the change of the trajectory on  $T_{90,i} - EH$  diagram, varying the shape of the GRB gamma-ray spectrum, and found only marginal change, following from the  $k$ -correction. Two another trajectories, representing famous type I GRB 170817A and type II GRB 130427A bursts, demonstrate the similar behavior (Fig. 6).

The blue curve, constructed for GRB 170817A, lies above the separation line  $EHD = 2.6$  in the whole considered range of redshift. Therefore, the burst can be classified as the type I one, even if the redshift is unknown. The closest point of the curve to the separation line is placed at  $z \approx 1.1$ , shown by plus symbol at Fig. 6. To conclude, if the value of  $EHD$  parameter is greater than 2.6 (the separation value) at  $z = 1.1$  for the investigated burst, one can classify it as the type I burst.

The red curve, constructed for GRB 130427A, is placed below the separation line at any considered redshift, indicating the burst to be from the type II population. So, if the value of  $EHD$  parameter is less than the separation value at the bounds of the considered redshift ( $z = 0.01$  and  $z = 10$  in our case), we can classify the burst (with no redshift measured) as the type II one.

In the intermediate region (e.g., as for GRB 060614A), when the trajectory crosses the separation line, we can not perform the classification, but we can restrict the possible redshift range of the source, if we know exactly the type of the burst from some other observational features (e.g. the absence of supernova and the presence of kilonova, as for GRB 060614A).

### 4.4 Comparison with several other classification methods based on combinations of $E_p$ , $E_{iso}$ and $T_{90,i}$

Attempts of using the combination of  $E_p$ ,  $E_{iso}$ ,  $T_{90,i}$  parameters and Amati relation as classification discriminators were made in several papers (e.g. Lü et al. 2010; Qin & Chen 2013; Zhang et al. 2018b; Shahmoradi & Nemiroff 2015; Zou et al. 2018; Pozanenko et al. 2018). Below we briefly compare the several classification schemes.

Lü et al. (2010) introduced a new classification parameter  $\epsilon = E_{iso,52}/E_{p,i,2}^k$ , which showed a clear bimodal distribution for  $k = 5/3$ . The value of power-law index  $k$  was not based on Amati relation and any other theoretical assumption, it was chosen just to minimize the dependence of  $\epsilon$  on redshift.

The  $\epsilon$  parameter is somewhat analogous to our  $EH$  parameter, being the power-law-like combination of  $E_p$  and  $E_{iso}$  parameters. As pointed out in Lü et al. (2010), it is not

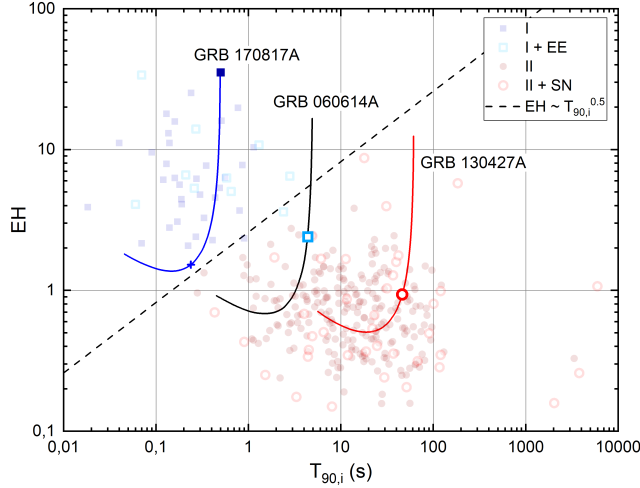


**Figure 6.** The  $T_{90,i} - EH$  diagram. The trajectories, representing the dependence of parameters on redshift, are shown for GRB 060614A by black curve, for GRB 170817A by blue curve, for GRB 130427A by red curve. The closest point of the blue curve to the separation line  $EHD = 2.6$  (dashed line) is shown by plus symbol. The diagram for I+EE bursts (cyan open squares), regular type I bursts (blue squares), II+SN bursts (red open circles) and type II (dark red circles) bursts is shown by semi-transparent symbols, except GRB 060614A, GRB 170817A and GRB 130427A.

obvious physically why the parameter  $\epsilon$  (corresponding to  $k = 5/3$ ) gives a cozy classification scheme. In that sense, the  $EH$  parameter has an advantage of being a direct consequence of Amati relation, although the nature of the Amati relation itself is still questionable.

The  $\epsilon$  parameter gives analogous to the  $EH$  parameter (but worse comparing with the  $EHD$ ) reliability of corresponding blind classification scheme, although the “problematic” GRB 060614A was classified correctly using  $\epsilon$ -based scheme. We should note, values of  $E_p$  and  $E_{iso}$  parameters for several common bursts, presented in both, our and Lü et al. (2010) samples differ significantly (e.g., for GRB 051221A and GRB 060801A). The reason of that discrepancy is not clear, the samples from both papers are mostly compilations of other papers.

Qin & Chen (2013) suggested the classification scheme, based directly on the  $E_{p,i} - E_{iso}$  correlation. They used the distribution of logarithmic deviation from the correlation of type II bursts  $\sigma = \lg E_{p,i} - \lg 94 - 0.57\lg E_{iso}$  to estimate the separation value. The deviation  $\sigma$  was firstly introduced in Amati (2006) to calculate the dispersion of the correlation of type II bursts. The classification method and the parameter  $\sigma$  are analogous to our  $EH$  scheme ( $\sigma \sim \lg EH$ ), except the power-law index value of Amati relation, which is  $a = 0.57$  in Qin & Chen (2013) and  $a = 0.4$  in our analysis. The discrepancy of power-law indices is connected at least with the difference of the samples: our sample contains three times more type I bursts and almost twice times more type II bursts. As we have shown in Section 3.1, fit parameters of the correlation also depend on the method used, which could be another reason of the discrepancy.

In Shahmoradi & Nemiroff (2015) the classification parameter  $R = E_p/T_{90}$  was proposed as least affected parameter by the detection threshold of gamma-ray detectors. It

was also suggested, that the two GRB types are most distinctively separated in the  $E_p - T_{90}$  plane. We check the classification scheme, based on the  $R$  parameter and its intrinsic equivalent ( $R_i = E_{p,i}/T_{90,i}$ ) for GRBs from our sample and found it to be similar with regular duration-based classification scheme. The result is connected with the fact, that the distributions of  $E_p$  and  $E_{p,i}$  for type I and type II GRBs are significantly overlapped with minor differences and give only marginal improvement in  $R$ -based scheme comparing with the duration-based one. But if we use instead of the  $E_{p,i}$  parameter the combination of  $E_{p,i}$  and  $E_{iso}$  parameters, following the bimodal nature of  $E_{p,i} - E_{iso}$  correlation, we obtain the  $EHD = R_i E_{iso}^{-0.4} T_{90,i}^{0.5} = E_{p,i} E_{iso}^{-0.4} T_{90,i}^{-0.5}$  parameter, giving the best separation of the type I / type II bursts of our sample.

## 5 CONCLUSIONS

We construct and investigate the most extensive (at the moment) sample of 45 type I and 275 type II gamma-ray bursts with a known redshift (both spectroscopic and photometric) and  $E_p$ . We discuss several selection effects, leading to the evolution of  $T_{90,i}$ ,  $E_{iso}$  and  $E_{p,i}$  parameters with redshift.

We confirm strong  $E_{p,i} - E_{iso}$  correlation for both types of bursts. The correlation for type I bursts is found to be well-distinguished from the one for type II bursts and has similar power-law index value,  $E_{p,i} \sim E_{iso}^{0.4}$ . It possibly indicates the same emission mechanism for both types.

Three possible outliers from the  $E_{p,i} - E_{iso}$  correlation for type II subsample are confirmed: GRB 980425B, GRB 031203A and GRB 171205A. They represent the subsample of the faintest type II bursts with  $E_{iso} < 10^{50}$  erg. The nature of their peculiarity and the behavior of the correlation at  $E_{iso} < 10^{50}$  erg remain unresolved. Increasing the sample of the faintest bursts could shed light on a problem.

We show that type I bursts with an extended emission and regular type I bursts follow the same correlation. It possibly indicates the same progenitor type for both subsamples of type I bursts. Nevertheless, I+EE bursts possibly form a separate sub-class of type I bursts, which is indicated by the features of redshift and duration distributions.

The same  $E_{p,i} - E_{iso}$  correlation behavior is also obtained for type II bursts with associated Ic supernovae and regular type II bursts, while the redshift,  $E_{p,i}$  and  $E_{iso}$  parameters distributions show significant differences. They are interpreted as strong selection effects, connected with observational constraints on supernova detection at a high redshift. It possibly indicates the same progenitor type for both subsamples of type II bursts, leading to the suggestion, that all type II bursts are accompanied by Ic supernovae.

The significant evolution of the  $E_{p,i} - E_{iso}$  correlation with redshift for type II bursts is not found. It confirms the weak selection effects on the correlation.

Using the  $E_{p,i} - E_{iso}$  correlation, we suggest two new classification methods by introducing two parameters,  $EH$  and  $EHD$ , representing the combination of the  $E_{p,i}$ ,  $E_{iso}$  and  $T_{90,i}$  parameters.  $EHD$  parameter is found to be the most reliable one for the GRB classification. It also can be used to classify bursts with no redshift or to estimate their redshift.

## ACKNOWLEDGEMENTS

Authors thank the anonymous referee for helpful suggestions and improvement of the paper. Authors acknowledge support from RSF grant 18-12-00378.

## REFERENCES

- Abbott B. P., et al., 2017a, *ApJ*, **848**, L12  
 Abbott B. P., et al., 2017b, *ApJ*, **848**, L13  
 Amati L., 2006, *MNRAS*, **372**, 233  
 Amati L., et al., 2002, *A&A*, **390**, 81  
 Barkov M. V., Pozanenko A. S., 2011, *MNRAS*, **417**, 2161  
 Barthelmy S. D., et al., 2012, GRB Coordinates Network, Circular Service, No. 13120, #1 (2012), [13120](#)  
 Belkin S., Pozanenko A., Mazaeva E., Volnova A., Minaev P., 2019a, in preparation  
 Belkin S., et al., 2019b, GRB Coordinates Network, Circular Service, No. 23601, #1 (2019), [23601](#)  
 Berger E., 2014, *ARA&A*, **52**, 43  
 Bernardini M. G., et al., 2015, *MNRAS*, **446**, 1129  
 Bhalerao V. B., Singer L. P., Kasliwal M. M., Cenko S. B., Horesh A., Perley D. A., 2014, GRB Coordinates Network, Circular Service, No. 16442, #1 (2014), [16442](#)  
 Blinnikov S. I., Novikov I. D., Perevodchikova T. V., Polnarev A. G., 1984, Soviet Astronomy Letters, **10**, 177  
 Bolmer J., Graham J., Knust F., Greiner J., 2015, GRB Coordinates Network, Circular Service, No. 18598, #1 (2015), [18598](#)  
 Butler N. R., Kocevski D., Bloom J. S., Curtis J. L., 2007, *ApJ*, **671**, 656  
 Cano Z., et al., 2011, *MNRAS*, **413**, 669  
 Cano Z., et al., 2014, *A&A*, **568**, A19  
 Cano Z., Malesani D., de Ugarte Postigo A., Izzo L., Thoene C. C., Castro-Rodriguez N., 2016, GRB Coordinates Network, Circular Service, No. 20245, #1 (2016), [20245](#)  
 Cano Z., Wang S.-Q., Dai Z.-G., Wu X.-F., 2017, *Advances in Astronomy*, **2017**, [8929054](#)  
 Castro-Tirado A. J., et al., 2014a, GRB Coordinates Network, Circular Service, No. 16505, #1 (2014), [16505](#)  
 Castro-Tirado A. J., Gorosabel J., Garcia-Rodriguez A., 2014b, GRB Coordinates Network, Circular Service, No. 16797, #1 (2014), [16797](#)  
 Castro-Tirado A., et al., 2019, GRB Coordinates Network, Circular Service, No. 23637, #1 (2019), [23708](#)  
 Cenko S. B., Prochaska J. X., Cucchiara A., Perley D. A., Bloom J. S., 2011, GRB Coordinates Network, Circular Service, No. 11736, #1 (2011), [11736](#)  
 Cenko S. B., et al., 2014, GRB Coordinates Network, Circular Service, No. 15883, #1 (2014), [15883](#)  
 Chornock R., Fong W., 2015, GRB Coordinates Network, Circular Service, No. 17358, #1 (2015), [17358](#)  
 Chornock R., Fox D. B., Berger E., 2014a, GRB Coordinates Network, Circular Service, No. 16269, #1 (2014), [16269](#)  
 Chornock R., Fox D. B., Cucchiara A., Perley D. A., Levan A., 2014b, GRB Coordinates Network, Circular Service, No. 16301, #1 (2014), [16301](#)  
 Cobb B. E., Bailyn C. D., van Dokkum P. G., Natarajan P., 2006, *ApJ*, **651**, L85  
 Connaughton V., 2002, *ApJ*, **567**, 1028  
 Cucchiara A., Fumagalli M., 2013, GRB Coordinates Network, Circular Service, No. 14207, #1 (2013), [14207](#)  
 Cucchiara A., Tanvir N. R., Perley D., Levan A. J., 2012, GRB Coordinates Network, Circular Service, No. 13512, #1 (2012), [13512](#)  
 Cummings J. R., et al., 2015, GRB Coordinates Network, Circular Service, No. 18580, #1 (2015), [18580](#)  
 D'Avanzo P., Heintz K., de Ugarte Postigo A., Levan A., Izzo L., Malesani D., Kann D., Tanvir N., 2018, GRB Coordinates Network, Circular Service, No. 23246, #1 (2018), [23246](#)  
 D'Elia V., et al., 2018, *A&A*, **619**, A66  
 Daigne F., Mochkovitch R., 2007, *A&A*, **465**, 1  
 Deming W. E., 2011, *Statistical Adjustment of Data* (Dover Books on Mathematics). Dover Publications  
 Dezaray J. P., Barat C., Talon R., Syunyaev R., Terekhov O., Kuznetsov A., 1992, in Paciesas W. S., Fishman G. J., eds, American Institute of Physics Conference Series Vol. 265, American Institute of Physics Conference Series. p. 304  
 Dezaray J.-P., et al., 1997, *ApJ*, **490**, L17  
 Donaghy T. Q., et al., 2006, ArXiv astro-ph/0605570,  
 Eichler D., Levinson A., 2004, *ApJ*, **614**, L13  
 Fenimore E. E., in 't Zand J. J. M., Norris J. P., Bonnell J. T., Nemiroff R. J., 1995, *ApJ*, **448**, L101  
 Fitzpatrick G., 2013, GRB Coordinates Network, Circular Service, No. 14896, #1 (2013), [14896](#)  
 Frederiks D., et al., 2016a, GRB Coordinates Network, Circular Service, No. 20059, #1 (2016), [20059](#)  
 Frederiks D., et al., 2016b, GRB Coordinates Network, Circular Service, No. 20082, #1 (2016), [20082](#)  
 Frederiks D., et al., 2016c, GRB Coordinates Network, Circular Service, No. 20111, #1 (2016), [20111](#)  
 Frederiks D., et al., 2017a, GRB Coordinates Network, Circular Service, No. 20604, #1 (2017), [20604](#)  
 Frederiks D., et al., 2017b, GRB Coordinates Network, Circular Service, No. 21247, #1 (2017), [21247](#)  
 Frederiks D., et al., 2017c, GRB Coordinates Network, Circular Service, No. 22003, #1 (2017), [22003](#)  
 Frederiks D., et al., 2018a, GRB Coordinates Network, Circular Service, No. 22546, #1 (2018), [22546](#)  
 Frederiks D., et al., 2018b, GRB Coordinates Network, Circular Service, No. 23061, #1 (2018), [23061](#)  
 Frederiks D., et al., 2018c, GRB Coordinates Network, Circular Service, No. 23240, #1 (2018), [23240](#)  
 Frederiks D., et al., 2018d, GRB Coordinates Network, Circular Service, No. 23424, #1 (2018), [23424](#)  
 Frontera F., et al., 2009, *ApJS*, **180**, 192  
 Galama T. J., et al., 1998, *Nature*, **395**, 670  
 Gehrels N., et al., 2006, *Nature*, **444**, 1044  
 Gendre B., Joyce Q. T., Orange N. B., Stratta G., Atteia J. L., Boë M., 2019, *MNRAS*, **486**, 2471  
 Ghirlanda G., Ghisellini G., Lazzati D., 2004, *ApJ*, **616**, 331  
 Ghirlanda G., Nava L., Ghisellini G., Celotti A., Firmani C., 2009, *A&A*, **496**, 585  
 Ghisellini G., Ghirlanda G., Mereghetti S., Bosnjak Z., Tavecchio F., Firmani C., 2006, *MNRAS*, **372**, 1699  
 Gibson S. L., Wynn G. A., Gompertz B. P., O'Brien P. T., 2017, *MNRAS*, **470**, 4925  
 Goldstein A., et al., 2017, *ApJ*, **848**, L14  
 Golenetskii S., et al., 2011, GRB Coordinates Network, Circular Service, No. 11722, #1 (2011), [11722](#)  
 Golenetskii S., et al., 2012, GRB Coordinates Network, Circular Service, No. 13736, #1 (2012), [13736](#)  
 Golenetskii S., et al., 2013a, GRB Coordinates Network, Circular Service, No. 14808, #1 (2013), [14808](#)  
 Golenetskii S., Aptekar R., Frederiks D., Pal'Shin V., Oleynik P., Ulanov M., Svinkin D., Cline T., 2013b, GRB Coordinates Network, Circular Service, No. 15260, #1 (2013), [15260](#)  
 Golenetskii S., Aptekar R., Frederiks D., Pal'Shin V., Oleynik P., Ulanov M., Svinkin D., Cline T., 2014a, GRB Coordinates Network, Circular Service, No. 15889, #1 (2014), [15889](#)  
 Golenetskii S., et al., 2014b, GRB Coordinates Network, Circular Service, No. 16374, #1 (2014), [16374](#)  
 Golenetskii S., et al., 2014c, GRB Coordinates Network, Circular Service, No. 16495, #1 (2014), [16495](#)  
 Golenetskii S., Aptekar R., Pal'Shin V., Frederiks D., Oleynik P.,

- Ulanov M., Svinkin D., Cline T., 2014d, GRB Coordinates Network, Circular Service, No. 17055, #1 (2014), [17055](#)
- Golenetskii S., et al., 2015a, GRB Coordinates Network, Circular Service, No. 17731, #1 (2015), [17731](#)
- Golenetskii S., et al., 2015b, GRB Coordinates Network, Circular Service, No. 18198, #1 (2015), [18198](#)
- Gorosabel J., de Ugarte Postigo A., Thoene C. C., Tanvir N., Fynbo J. P. U., Garcia-Alvarez D., Perez-Romero A., 2014, GRB Coordinates Network, Circular Service, No. 17234, #1 (2014), [17234](#)
- Gruber D., 2012, GRB Coordinates Network, Circular Service, No. 13469, #1 (2012), [13469](#)
- Guetta D., Piran T., 2005, *A&A*, **435**, 421
- Hakkila J., Preece R. D., 2011, *ApJ*, **740**, 104
- Hakkila J., Giblin T. W., Norris J. P., Fragile P. C., Bonnell J. T., 2008, *ApJ*, **677**, L81
- Hartoog O. E., Xu D., Malesani D., Tanvir N. R., Fynbo J. P. U., Kaper L., D'Elia V., 2013, GRB Coordinates Network, Circular Service, No. 15494, #1 (2013), [15494](#)
- Heussaff V., Atteia J. L., Zolnierowski Y., 2013, *A&A*, **557**, A100
- Hjorth J., et al., 2003, *Nature*, **423**, 847
- Ito H., Matsumoto J., Nagataki S., Warren D. C., Barkov M. V., Yonetoku D., 2019, *Nature Communications*, **10**, 1504
- Izzo L., et al., 2018a, GRB Coordinates Network, Circular Service, No. 22567, #1 (2018/March-0), [22567](#)
- Izzo L., et al., 2018b, GRB Coordinates Network, Circular Service, No. 22823, #1 (2018), [22823](#)
- Izzo L., et al., 2018c, GRB Coordinates Network, Circular Service, No. 23488, #1 (2018/December-0), [23488](#)
- Jenke P., Fitzpatrick G., 2014, GRB Coordinates Network, Circular Service, No. 15923, #1 (2014), [15923](#)
- Jeong S., Sanchez-Ramirez R., Gorosabel J., Castro-Tirado A. J., 2014, GRB Coordinates Network, Circular Service, No. 15936, #1 (2014), [15936](#)
- Jin Z.-P., Fan Y.-Z., Wei D.-M., 2016, in European Physical Journal Web of Conferences. p. 08002 ([arXiv:1512.04192](#)), doi:[10.1051/epjconf/201610908002](#)
- Kann D. A., et al., 2011, *ApJ*, **734**, 96
- Kasliwal M. M., Cenko S. B., Singer L. P., 2014, GRB Coordinates Network, Circular Service, No. 16425, #1 (2014), [16425](#)
- Knust F., Kruehler T., Klose S., Greiner J., 2012, GRB Coordinates Network, Circular Service, No. 13810, #1 (2012), [13810](#)
- Kouveliotou C., Meegan C. A., Fishman G. J., Bhat N. P., Briggs M. S., Koshut T. M., Paciesas W. S., Pendleton G. N., 1993, *ApJ*, **413**, L101
- Krimm H. A., et al., 2012a, GRB Coordinates Network, Circular Service, No. 13517, #1 (2012), [13517](#)
- Krimm H. A., et al., 2012b, GRB Coordinates Network, Circular Service, No. 13634, #1 (2012), [13634](#)
- Krimm H. A., et al., 2013, GRB Coordinates Network, Circular Service, No. 15499, #1 (2013), [15499](#)
- Kruehler T., Schady P., Greiner J., Tanvir N. R., 2017, GRB Coordinates Network, Circular Service, No. 20686, #1 (2017), [20686](#)
- Krühler T., et al., 2015, *A&A*, **581**, A125
- Kulkarni S. R., et al., 1998, *Nature*, **395**, 663
- Lazzati D., Ramirez-Ruiz E., Ghisellini G., 2001, *A&A*, **379**, L39
- Levinson A., Eichler D., 2005, *ApJ*, **629**, L13
- Lloyd N. M., Petrosian V., Mallozzi R. S., 2000, *ApJ*, **534**, 227
- Lü H.-J., Liang E.-W., Zhang B.-B., Zhang B., 2010, *ApJ*, **725**, 1965
- Malesani D., et al., 2014, GRB Coordinates Network, Circular Service, No. 15800, #1 (2014), [15800](#)
- Mallozzi R. S., Paciesas W. S., Pendleton G. N., Briggs M. S., Preece R. D., Meegan C. A., Fishman G. J., 1995, *ApJ*, **454**, 597
- Markwardt C. B., et al., 2009, GRB Coordinates Network, Circular Service, No. 1040, #1 (2009), [10040](#)
- Markwardt C. B., et al., 2017, GRB Coordinates Network, Circular Service, No. 20456, #1 (2017), [20456](#)
- Mazaeva E., Klunko E., Volnova A., Korobtsev I., Pozanenko A., 2015, GRB Coordinates Network, Circular Service, No. 18205, #1 (2015), [18205](#)
- Mazets E. P., et al., 1981, *Ap&SS*, **80**, 3
- Melandri A., et al., 2019, GRB Coordinates Network, Circular Service, No. 23983, #1 (2019/March-0), [23983](#)
- Mészáros P., 2006, *Reports on Progress in Physics*, **69**, 2259
- Meszárás P., Rees M. J., 1992, *ApJ*, **397**, 570
- Metzger B. D., Quataert E., Thompson T. A., 2008, *MNRAS*, **385**, 1455
- Minaev P. Y., Pozanenko A. S., 2017, *Astronomy Letters*, **43**, 1
- Minaev P. Y., Pozanenko A. S., Loznikov V. M., 2010a, *Astronomy Letters*, **36**, 707
- Minaev P. Y., Pozanenko A. S., Loznikov V. M., 2010b, *Astrophysical Bulletin*, **65**, 326
- Minaev P. Y., Grebenev S. A., Pozanenko A. S., Molkov S. V., Frederiks D. D., Golenetskii S. V., 2012, *Astronomy Letters*, **38**, 613
- Minaev P. Y., Pozanenko A. S., Molkov S. V., Grebenev S. A., 2014, *Astronomy Letters*, **40**, 235
- Montanari E., Frontera F., Guidorzi C., Rapisarda M., 2005, *ApJ*, **625**, L17
- Narayana Bhat P., et al., 2016, *ApJS*, **223**, 28
- Nava L., et al., 2012, *MNRAS*, **421**, 1256
- Norris J. P., 2002, *ApJ*, **579**, 386
- Norris J. P., Bonnell J. T., 2006, *ApJ*, **643**, 266
- Norris J. P., Marani G. F., Bonnell J. T., 2000, *ApJ*, **534**, 248
- Norris J. P., Bonnell J. T., Kazanas D., Scargle J. D., Hakkila J., Giblin T. W., 2005, *ApJ*, **627**, 324
- Norris J. P., Gehrels N., Scargle J. D., 2010, *ApJ*, **717**, 411
- Norris J. P., Barthelmy S. D., Cummings J. R., Gehrels N., 2015, GRB Coordinates Network, Circular Service, No. 17759, #1 (2015), [17759](#)
- Paczynski B., 1986, *ApJ*, **308**, L43
- Paczynski B., 1998, *ApJ*, **494**, L45
- Pal'Shin V., et al., 2013, GRB Coordinates Network, Circular Service, No. 14702, #1 (2013), [14702](#)
- Palmer D. M., et al., 2016, GRB Coordinates Network, Circular Service, No. 20308, #1 (2016), [20308](#)
- Palmer D. M., et al., 2018, GRB Coordinates Network, Circular Service, No. 22566, #1 (2018/March-0), [22566](#)
- Pandey S. B., et al., 2019, *MNRAS*, **485**, 5294
- Pelassa V., 2014, GRB Coordinates Network, Circular Service, No. 16900, #1 (2014), [16900](#)
- Perley D. A., Cao Y., Cenko S. B., 2014, GRB Coordinates Network, Circular Service, No. 17228, #1 (2014), [17228](#)
- Planck Collaboration et al., 2014, *A&A*, **571**, A16
- Pozanenko A. S. e. a., 2019, in preparation
- Pozanenko A. S., et al., 2018, *ApJ*, **852**, L30
- Pozanenko A., Minaev P., Barkov M., Warren D., 2019a, in preparation
- Pozanenko A. S., Minaev P. Y., Grebenev S. A., Chelovekov I. V., 2019b, *Astronomy Letters*, **45**, 768
- Qin Y.-P., Chen Z.-F., 2013, *MNRAS*, **430**, 163
- Rau A., Kruehler T., Greiner J., 2013, GRB Coordinates Network, Circular Service, No. 15330, #1 (2013), [15330](#)
- Rosswog S., 2007, *MNRAS*, **376**, L48
- Rosswog S., Ramirez-Ruiz E., 2003, *MNRAS*, **343**, L36
- Sakamoto T., et al., 2016a, GRB Coordinates Network, Circular Service, No. 19106, #1 (2016), [19106](#)
- Sakamoto T., et al., 2016b, GRB Coordinates Network, Circular Service, No. 19276, #1 (2016), [19276](#)
- Savchenko V., et al., 2017, *ApJ*, **848**, L15
- Schaefer B. E., 2007, *ApJ*, **660**, 16
- Selsing J., et al., 2018, *A&A*, **616**, A48
- Shahmoradi A., Nemiroff R. J., 2015, *MNRAS*, **451**, 126

- Smette A., Ledoux C., Vreeswijk P., De Cia A., Petitjean P., Fynbo J., Malesani D., Fox A., 2013, GRB Coordinates Network, Circular Service, No. 14848, #1 (2013), [14848](#)
- Stamatikos M., et al., 2014, GRB Coordinates Network, Circular Service, No. 16284, #1 (2014), [16284](#)
- Stamatikos M., et al., 2015, GRB Coordinates Network, Circular Service, No. 18527, #1 (2015), [18527](#)
- Svinkin D. S., et al., 2016a, *ApJS*, **224**, 10
- Svinkin D., et al., 2016b, GRB Coordinates Network, Circular Service, No. 20197, #1 (2016), [20197](#)
- Svinkin D., et al., 2017, GRB Coordinates Network, Circular Service, No. 21299, #1 (2017), [21299](#)
- Svinkin D., et al., 2018, GRB Coordinates Network, Circular Service, No. 23495, #1 (2018/December-0), [23495](#)
- Tanaka M., 2016, *Advances in Astronomy*, **2016**, 634197
- Tanvir N. R., Wiersema K., Xu D., Fynbo J. P. U., 2013, GRB Coordinates Network, Circular Service, No. 14882, #1 (2013), [14882](#)
- Tanvir N. R., Levan A. J., Wiersema K., Petric A., Chiboucas K., Miller J., 2014, GRB Coordinates Network, Circular Service, No. 16150, #1 (2014), [16150](#)
- Tanvir N. R., Xu D., Zafar T., Covino S., Schulze S., 2015a, GRB Coordinates Network, Circular Service, No. 18080, #1 (2015), [18080](#)
- Tanvir N. R., Kruehler T., Malesani D., Xu D., de Ugarte Postigo A., Pugliese G., 2015b, GRB Coordinates Network, Circular Service, No. 18524, #1 (2015), [18524](#)
- Tanvir N. R., Kruehler T., Wiersema K., Xu D., Malesani D., Milvang-Jensen B., Fynbo J. P. U., 2016, GRB Coordinates Network, Circular Service, No. 20321, #1 (2016), [20321](#)
- Tanvir N. R., et al., 2018, GRB Coordinates Network, Circular Service, No. 22384, #1 (2018/February-0), [22384](#)
- Tarnopolski M., 2016, *MNRAS*, **458**, 2024
- Tello J. C., Sanchez-Ramirez R., Gorosabel J., Castro-Tirado A. J., Rivero M. A., Gomez-Velarde G., Klotz A., 2012, GRB Coordinates Network, Circular Service, No. 13118, #1 (2012), [13118](#)
- Thoene C. C., de Ugarte Postigo A., Gorosabel J., Sanchez-Ramirez R., Fynbo J. P. U., Gomez Velarde G., 2012, GRB Coordinates Network, Circular Service, No. 13628, #1 (2012), [13628](#)
- Tremaine S., et al., 2002, *ApJ*, **574**, 740
- Tsvetkova A., et al., 2017, *ApJ*, **850**, 161
- Tsvetkova A., et al., 2018, GRB Coordinates Network, Circular Service, No. 23363, #1 (2018), [23363](#)
- Tsvetkova A., et al., 2019, GRB Coordinates Network, Circular Service, No. 23637, #1 (2019), [23637](#)
- Tueller J., et al., 2008, GRB Coordinates Network, [7205](#)
- Ukwatta T. N., et al., 2012, *MNRAS*, **419**, 614
- Ukwatta T. N., et al., 2014, GRB Coordinates Network, Circular Service, No. 16306, #1 (2014), [16306](#)
- Volnova A. A., et al., 2014, *MNRAS*, **442**, 2586
- Volnova A. A., et al., 2017, *MNRAS*, **467**, 3500
- Vreeswijk P. M., et al., 2018, GRB Coordinates Network, Circular Service, No. 22996, #1 (2018), [22996](#)
- Woosley S. E., 1993, *ApJ*, **405**, 273
- Xu D., Fynbo J. P. U., D'Elia V., Tanvir N. R., 2012, GRB Coordinates Network, Circular Service, No. 13460, #1 (2012), [13460](#)
- Xu D., Levan A. J., Fynbo J. P. U., Tanvir N. R., D'Elia V., Malesani D., 2014, GRB Coordinates Network, Circular Service, No. 16983, #1 (2014), [16983](#)
- Xu D., Fynbo J. P. U., Malesani D., de Ugarte Postigo A., Petrushevska T., Saario J., Telting J., 2016a, GRB Coordinates Network, Circular Service, No. 19109, #1 (2016), [19109](#)
- Xu D., Heintz K. E., Malesani D., Wiersema K., Fynbo J. P. U., 2016b, GRB Coordinates Network, Circular Service, No. 19773, #1 (2016), [19773](#)
- Xu D., Heintz K. E., Malesani D., Fynbo J. P. U., 2017, GRB Coordinates Network, Circular Service, No. 20458, #1 (2017), [20458](#)
- Yang B., et al., 2015, *Nature Communications*, **6**, 7323
- Yi T., Liang E., Qin Y., Lu R., 2006, *MNRAS*, **367**, 1751
- Yonetoku D., Murakami T., Nakamura T., Yamazaki R., Inoue A. K., Ioka K., 2004, *ApJ*, **609**, 935
- York D., Evensen N. M., Martinez M. L., De Basabe Delgado J., 2004, *American Journal of Physics*, **72**, 367
- Younes G., Bhat P. N., 2013, GRB Coordinates Network, Circular Service, No. 14219, #1 (2013), [14219](#)
- Zhang Z., Xie G. Z., Deng J. G., Jin W., 2006, *MNRAS*, **373**, 729
- Zhang B., et al., 2009, *ApJ*, **703**, 1696
- Zhang F.-W., Shao L., Yan J.-Z., Wei D.-M., 2012, *ApJ*, **750**, 88
- Zhang B.-B., et al., 2018a, *Nature Astronomy*, **2**, 69
- Zhang Z. B., Zhang C. T., Zhao Y. X., Luo J. J., Jiang L. Y., Wang X. L., Han X. L., Terheide R. K., 2018b, *PASP*, **130**, 054202
- Zou Y.-C., Wang F.-F., Moharana R., Liao B., Chen W., Wu Q., Lei W.-H., Wang F.-Y., 2018, *ApJ*, **852**, L1
- de Ugarte Postigo A., Tanvir N., Sanchez-Ramirez R., Thoene C. C., Gorosabel J., Fynbo J. P. U., 2013, GRB Coordinates Network, Circular Service, No. 14437, #1 (2013), [14437](#)
- de Ugarte Postigo A., et al., 2014, GRB Coordinates Network, Circular Service, No. 16902, #1 (2014), [16902](#)
- de Ugarte Postigo A., Kruehler T., Flores H., Fynbo J. P. U., 2015, GRB Coordinates Network, Circular Service, No. 17523, #1 (2015), [17523](#)
- de Ugarte Postigo A., et al., 2016, GRB Coordinates Network, Circular Service, No. 20342, #1 (2016), [20342](#)
- de Ugarte Postigo A., Izzo L., Thoene C. C., Cano Z., Kann D. A., Scarpa R., Herrera V., 2017a, GRB Coordinates Network, Circular Service, No. 21240, #1 (2017), 21240
- de Ugarte Postigo A., Kann D. A., Izzo L., Thoene C. C., 2017b, GRB Coordinates Network, Circular Service, No. 21298, #1 (2017), [21298](#)
- de Ugarte Postigo A., Izzo L., Thoene C. C., Kann D. A., Heintz K. E., Castro-Rodriguez N., Marante A., 2017c, GRB Coordinates Network, Circular Service, No. 21799, #1 (2017), [21799](#)
- de Ugarte Postigo A., et al., 2017d, GRB Coordinates Network, Circular Service, No. 22096, #1 (2017), [22096](#)
- de Ugarte Postigo A., Izzo L., Kann D. A., Thoene C. C., Peshev P., Scarpa R., Perez D., 2017e, GRB Coordinates Network, Circular Service, No. 22204, #1 (2017), [22204](#)
- de Ugarte Postigo A., Izzo L., Kann D. A., Thoene C. C., Perley D. A., Malesani D., Heintz K. E., Garcia D., 2017f, GRB Coordinates Network, Circular Service, No. 22272, #1 (2017), [22272](#)
- von Kienlin A., 2018, GRB Coordinates Network, Circular Service, No. 22386, #1 (2018/February-0), [22386](#)
- von Kienlin A., Burns E., 2015, GRB Coordinates Network, Circular Service, No. 17319, #1 (2015), [17319](#)

## APPENDIX A: THE SAMPLE OF GAMMA-RAY BURSTS

Table A contains observational parameters of the GRB sample.

This paper has been typeset from a Te<sub>X</sub>/La<sub>T</sub>E<sub>X</sub> file prepared by the author.

**Table A1.** The sample of gamma-ray bursts.

GRB	$T_{90,i}$ <sup>a</sup> s	$z$ <sup>b</sup>	$E_{iso}$ $10^{51}$ erg	$E_{p,i}$ keV	Type <sup>c</sup>	Experiment <sup>d</sup>	Refs <sup>e</sup>	$EH$	Type <sup>f</sup>	$EHD$	Type <sup>g</sup>
970228	31.5	0.695	$12.01 \pm 0.93$	$280^{+66}_{-42}$	II+SNph	Konus-Wind	1; 2	1.04	II	0.19	II
970508	10.9	0.835	$6.12 \pm 1.30$	$145^{+43}_{-43}$	II	BeppoSAX	3	0.70	II	0.21	II
970828	33.8	0.9578	$262.2 \pm 9.1$	$531^{+47}_{-43}$	II	Konus-Wind	1	0.57	II	0.10	II
971214	3.6	3.418	$146.3 \pm 6.1$	$791^{+88}_{-71}$	II	Konus-Wind	1	1.08	II	0.57	II
980326	4.5	1 PH	$4.82 \pm 0.90$	$71 \pm 36$	II+SNph	BeppoSAX	2; 3	0.38	II	0.18	II
980425B	17.9	0.0085	$0.0010 \pm 0.0002$	$55 \pm 21$	II+SNsp	BATSE/CGRO	2; 4	8.72	I	2.06	II
980613	9.5	1.096	$5.9 \pm 0.9$	$194 \pm 89$	II	BeppoSAX	3	0.95	II	0.31	II
980703	52.1	0.966	$72 \pm 7$	$503 \pm 64$	II	BATSE/CGRO	3	0.91	II	0.13	II
990123	23.9	1.6004	$2133 \pm 54$	$1883^{+88}_{-81}$	II	Konus-Wind	1	0.88	II	0.18	II
990506	55.8	1.30658	$1255 \pm 43$	$683^{+62}_{-58}$	II	Konus-Wind	1	0.39	II	0.05	II
990510	21.3	1.6187	$174.2 \pm 8.1$	$356^{+39}_{-26}$	II	Konus-Wind	1	0.45	II	0.10	II
990705	18.0	0.8424	$218.1 \pm 7.7$	$551 \pm 17$	II	Konus-Wind	1	0.64	II	0.15	II
990712	11.6	0.4331	$3.86 \pm 0.28$	$149^{+21}_{-16}$	II+SNph	Konus-Wind	1; 2	0.87	II	0.26	II
991208	37.0	0.7055	$233.4 \pm 4.6$	$315.5 \pm 8.5$	II+SNph	Konus-Wind	1; 2	0.36	II	0.06	II
991216	7.2	1.02	$886 \pm 11$	$713 \pm 30$	II	Konus-Wind	1	0.47	II	0.18	II
000131	17.5	4.5	$1817 \pm 11$	$732^{+72}_{-66}$	II	Konus-Wind	1	0.36	II	0.09	II
000210	4.32	0.8463	$193.1 \pm 4.8$	$687^{+39}_{-37}$	II	Konus-Wind	1	0.84	II	0.40	II
000301C	1.21	2.0335	$33.7 \pm 5.0$	$494^{+200}_{-109}$	II	Konus-Wind	1	1.21	II	1.10	II
000418	13.1	1.1181	$95.7 \pm 4.9$	$246^{+21}_{-17}$	II	Konus-Wind	1	0.40	II	0.11	II
000911	11.3	1.0585	$649 \pm 20$	$2229^{+107}_{-103}$	II+SNph	Konus-Wind	1; 2	1.67	II	0.50	II
000926A	18.0	2.0369	$278 \pm 11$	$328^{+24}_{-21}$	II	Konus-Wind	1	0.35	II	0.08	II
010222	36.2	1.4768	$1072 \pm 30$	$706^{+34}_{-50}$	II	Konus-Wind	1	0.43	II	0.07	II
010921	13.7	0.45	$10.84 \pm 0.47$	$135^{+12}_{-10}$	II	Konus-Wind	1	0.52	II	0.14	II
011121	41.9	0.36	$98.9 \pm 2.7$	$1114^{+147}_{-131}$	II+SNsp	Konus-Wind	1; 2	1.77	II	0.27	II
011211	16.2	2.14	$63 \pm 7$	$186 \pm 24$	II	BeppoSAX	4; 5	0.36	II	0.09	II
020124	18.7	3.198	$270 \pm 30$	$448 \pm 148$	II	HETE-2	3	0.48	II	0.11	II
020127	6.1	1.9 <sup>+0.2</sup> <sub>-0.4</sub> PH	$35 \pm 1$	$290 \pm 100$	II	HETE-2	3	0.70	II	0.28	II
020405	24.6	0.6898	$117.3 \pm 1.8$	$272 \pm 12$	II+SNph	Konus-Wind	1; 2	0.40	II	0.08	II
020813	39.7	1.254	$758 \pm 47$	$512^{+41}_{-38}$	II	Konus-Wind	1	0.36	II	0.06	II
020819B	5.8	0.411	$3.51 \pm 0.39$	$224^{+89}_{-40}$	II	Konus-Wind	1	1.36	II	0.56	II
020903	8.0	0.25	$0.024 \pm 0.006$	$3.37 \pm 1.79$	II+SNph	HETE-2	2; 3	0.15	II	0.05	II
021004	23.4	2.33	$33 \pm 4$	$266 \pm 117$	II	HETE-2	3	0.66	II	0.14	II
021211	0.9	1.004	$9.9 \pm 1.9$	$108^{+26}_{-50}$	II+SNsp	Konus-Wind	1; 2	0.43	II	0.46	II
030226	25.8	1.98	$121 \pm 13$	$289 \pm 66$	II	HETE-2	3	0.42	II	0.08	II
030323	7.46	3.372	$28 \pm 9$	$270 \pm 113$	II	HETE-2	3	0.71	II	0.26	II
030328	55.6	1.52	$470 \pm 30$	$328 \pm 55$	II	HETE-2	3	0.28	II	0.04	II
030329	18.7	0.16854	$16.55 \pm 0.30$	$113.3 \pm 2.3$	II+SNsp	Konus-Wind	1; 2	0.37	II	0.09	II
030429	2.8	2.65	$21.6 \pm 2.6$	$128 \pm 26$	II	HETE-2	3	0.37	II	0.22	II
030528	27.6	0.782	$25 \pm 3$	$57 \pm 9$	II	HETE-2	3	0.16	II	0.03	II
031203	31.0	0.105	$0.10 \pm 0.04$	$158 \pm 51$	II+SNsp	Konus-Wind	2; 4; 6	3.97	I	0.71	II
040912	55.8	1.563	$13 \pm 3$	$44 \pm 33$	II	HETE-2	3	0.16	II	0.02	II
040924	0.43	0.859	$5.08 \pm 0.27$	$133.8 \pm 11.2$	II+SNph	Konus-Wind	1; 2	0.70	II	1.07	II
041006	4.0	0.716	$6.88 \pm 0.37$	$147.6 \pm 8.6$	II+SNph	Konus-Wind	1; 2	0.68	II	0.34	II
050126A	10.8	1.29	$7.36 \pm 1.60$	$263 \pm 110$	II	Swift	3	1.18	II	0.36	II
050223	14.1	0.5915	$1.21 \pm 0.18$	$110 \pm 54$	II	Swift	3	1.02	II	0.27	II
050318	13.1	1.44	$22 \pm 1.6$	$115 \pm 25$	II	Swift	3	0.33	II	0.09	II
050401	8.5	2.8992	$464 \pm 22$	$409^{+55}_{-43}$	II	Konus-Wind	1	0.35	II	0.12	II
050416A	1.52	0.6535	$1.0 \pm 0.1$	$25.1 \pm 4.2$	II+SNph	Swift	2; 3	0.25	II	0.20	II
050505	11.2	4.27	$176.0 \pm 26.1$	$661 \pm 245$	II	Swift	3	0.84	II	0.25	II
050509B	0.04	0.2248	$0.0024^{+0.0044}_{-0.0010}$	$100^{+748}_{-98}$	I	Swift	7	11.2	I	55.8	I
050525A	4.4	0.606	$28.08 \pm 0.61$	$128.5 \pm 3.2$	II+SNsp	Konus-Wind	1; 2	0.34	II	0.16	II
050603	2.9	2.821	$947 \pm 63$	$913^{+245}_{-130}$	II	Konus-Wind	1	0.59	II	0.35	II
050709A	0.06	0.1606	$0.027 \pm 0.011$	$96.3^{+20.9}_{-13.9}$	I+EE	HETE-2	7	4.08	I	16.7	I
050724A	2.4	0.2576	$0.09^{+0.11}_{-0.02}$	$138^{+503}_{-57}$	I+EE	Swift	7; 8	3.62	I	2.33	II
050803	61.8	0.422	$1.86 \pm 0.40$	$138 \pm 48$	II	Swift	3	1.08	II	0.14	II
050813A	0.35	0.72	$0.15^{+0.25}_{-0.08}$	$361^{+1221}_{-224}$	I	Swift	7	7.71	I	13.0	I
050814	24.0	5.3 <sup>+0.3</sup> <sub>-0.3</sub> PH	$112.0 \pm 24.3$	$339 \pm 47$	II	Swift	3	0.51	II	0.11	II
050820	122	2.6147	$1036 \pm 36$	$1753^{+539}_{-333}$	II	Konus-Wind	1	1.09	II	0.10	II
050904	23.9	6.29	$1240 \pm 130$	$3178 \pm 1094$	II	Swift	3	1.84	II	0.38	II
050908	4.5	3.344	$19.7 \pm 3.2$	$195 \pm 36$	II	Swift	3	0.59	II	0.28	II

**Table A1 – continued**

GRB	$T_{90,i}$ s	$z$	$E_{\text{iso}}$ $10^{51}$ erg	$E_{\text{p},i}$ keV	Type	Experiment	Refs	<i>EH</i> Type	<i>EHD</i> Type
050922C	2.0	2.198	$53 \pm 17$	$415 \pm 111$	II	HETE-2	3	0.85 II	0.60 II
051008	55.4	$2.77^{+0.15}_{-0.20}$ PH	$834 \pm 70$	$2074^{+501}_{-354}$	II	Konus-Wind	1; 9	1.41 II	0.19 II
051022	85.4	0.8	$490 \pm 10$	$794^{+32}_{-29}$	II	Konus-Wind	1	0.67 II	0.07 II
051109A	11.9	2.346	$71.1 \pm 8.5$	$569^{+268}_{-141}$	II	Konus-Wind	1	1.03 II	0.30 II
051221A	0.14	0.5465	$9.10^{+1.29}_{-1.12}$	$677^{+200}_{-141}$	I	Konus-Wind	10	2.80 II	7.48 I
060115	30.8	3.53	$63 \pm 9$	$285 \pm 34$	II	Swift	3	0.54 II	0.10 II
060121	0.28	$4.6 \pm 0.5$ PH	$180 \pm 12$	$767^{+84}_{-67}$	II	Konus-Wind	1	0.96 II	1.82 II
060124	72.2	2.297	$328 \pm 15$	$788^{+62}_{-86}$	II	Konus-Wind	1; 3	0.78 II	0.09 II
060206	1.51	4.048	$43 \pm 9$	$394 \pm 46$	II	Swift	3	0.88 II	0.71 II
060210	51.9	3.91	$415.3 \pm 57.0$	$575 \pm 186$	II	Swift	3	0.52 II	0.07 II
060218	2033	0.0331	$0.053 \pm 0.003$	$4.9 \pm 0.3$	II+SNsp	Swift	2; 3	0.16 II	0.004 II
060223A	2.09	4.41	$42.9 \pm 6.6$	$339 \pm 63$	II	Swift	3	0.75 II	0.52 II
060306*	23.8	1.5597	$20.3^{+7.0}_{-3.2}$	$171^{+79}_{-41}$	II	Swift	11; 12	0.51 II	0.11 II
060418	41.4	1.489	$130 \pm 30$	$572 \pm 143$	II	Konus-Wind	3	0.82 II	0.13 II
060502A	4.2	1.5026	$23.4 \pm 2.9$	$320^{+115}_{-63}$	II	Konus-Wind	1	0.91 II	0.44 II
060502B	0.12	0.287	$0.433 \pm 0.053$	$438^{+561}_{-148}$	I	Swift	13	6.12 I	17.7 I
060510B	46.6	4.94	$367.0 \pm 28.7$	$575 \pm 227$	II	Swift	3	0.54 II	0.08 II
060522	11.6	5.11	$77.7 \pm 15.2$	$427 \pm 79$	II	Swift	3	0.75 II	0.22 II
060526	70.8	3.221	$26 \pm 3$	$105 \pm 21$	II	Swift	3	0.29 II	0.03 II
060605	16.6	3.78	$28.3 \pm 4.5$	$490 \pm 251$	II	Swift	3	1.29 II	0.32 II
060607A	25.0	3.075	$109.0 \pm 15.5$	$575 \pm 200$	II	Swift	3	0.88 II	0.18 II
060614A	4.4	0.1254	$2.4 \pm 0.4$	$340^{+241}_{-96}$	I+EE	Swift	1; 7; 8	2.40 II	1.14 II
060707	14.9	3.425	$54 \pm 10$	$279^{+28}_{-28}$	II	Swift	3	0.57 II	0.15 II
060714	31.0	2.711	$134 \pm 9$	$234 \pm 109$	II	Swift	3	0.33 II	0.06 II
060801A	0.33	1.131	$32.7 \pm 4.9$	$1321^{+1379}_{-439}$	I	Swift	13	3.27 II	5.70 I
060814	49.9	1.9229	$414 \pm 25$	$1257^{+1055}_{-371}$	II	Konus-Wind	1	1.13 II	0.16 II
060904B	100.7	0.703	$3.64 \pm 0.74$	$135 \pm 41$	II+SNph	Swift	2; 3	0.81 II	0.08 II
060906	9.3	3.686	$149.0 \pm 15.6$	$209 \pm 43$	II	Swift	3	0.28 II	0.09 II
060908	5.6	2.43	$98 \pm 9$	$514 \pm 102$	II	Swift	3	0.82 II	0.35 II
060912A	2.5	0.937	$11.7 \pm 3.3$	$395^{+589}_{-145}$	II	Konus-Wind	1	1.48 II	0.93 II
060927	3.4	5.47	$138 \pm 20$	$475^{+47}_{-47}$	II	Swift	3	0.66 II	0.36 II
061006A	0.26	0.4377	$3.82^{+0.73}_{-0.63}$	$909^{+260}_{-191}$	I+EE	Konus-Wind	8; 10	5.32 I	10.4 I
061007	25.5	1.261	$1113 \pm 40$	$902^{+27}_{-25}$	II	Konus-Wind	1	0.55 II	0.11 II
061021	13.9	0.3453	$4.53 \pm 0.88$	$702^{+357}_{-187}$	II	Konus-Wind	1	3.84 I	1.03 II
061121	7.7	1.314	$304 \pm 11$	$1405^{+120}_{-106}$	II	Konus-Wind	1	1.43 II	0.51 II
061126	32.8	1.1588	$300 \pm 30$	$1337 \pm 410$	II	Swift	3	1.37 II	0.24 II
061201A	0.77	0.111	$0.168 \pm 0.029$	$970^{+298}_{-209}$	I	Konus-Wind	1	19.8 I	22.6 I
061210A	0.07	0.4095	$0.024 \pm 0.006$	$761^{+648}_{-364}$	I+EE	Swift	8; 13	33.8 I	127.9 I
061217A	0.19	0.827	$4.23 \pm 0.72$	$731^{+895}_{-287}$	I	Swift	13	4.11 I	9.42 I
061222A	19.5	2.088	$259.9 \pm 6.8$	$920^{+80}_{-68}$	II	Konus-Wind	1	1.00 II	0.23 II
061222B	9.2	3.355	$103 \pm 16$	$200 \pm 28$	II	Swift	3	0.31 II	0.10 II
070110	26.4	2.352	$55 \pm 15$	$370 \pm 170$	II	Swift	3	0.75 II	0.15 II
070125	48.8	1.547	$1278 \pm 64$	$947^{+92}_{-79}$	II	Konus-Wind	1	0.54 II	0.08 II
070328	17.6	2.0627	$777 \pm 85$	$1182^{+181}_{-144}$	II	Konus-Wind	1	0.83 II	0.20 II
070429B	0.17	0.904	$0.475 \pm 0.071$	$229^{+859}_{-76}$	I	Swift	13	3.08 II	7.48 I
070508	8.1	0.82	$79.8 \pm 1.2$	$342.2^{+9.1}_{-7.3}$	II	Konus-Wind	1	0.59 II	0.21 II
070521	11.8	2.0865	$147.5 \pm 4.6$	$589^{+43.3}_{-38}$	II	Konus-Wind	1; 12	0.80 II	0.23 II
070714B	0.65	0.923	$6.4 \pm 1.1$	$1060^{+285}_{-215}$	I+EE	Konus-Wind	1; 8	5.05 I	6.26 I
070724A	0.27	0.457	$0.016 \pm 0.003$	$119.5 \pm 7.3$	I	Swift	14	6.21 I	11.84 I
070729A	0.56	0.8 PH	$1.13 \pm 0.44$	$666^{+675}_{-261}$	I	Swift	13	6.34 I	8.48 I
070809	0.44	2.187	$1.04 \pm 0.16$	$464 \pm 223$	I	Swift	14	4.57 I	6.92 I
071003	8.2	1.60435	$385 \pm 18$	$2086^{+188}_{-164}$	II	Konus-Wind	1	1.93 II	0.67 II
071010B	4.4	0.947	$14.5 \pm 1.3$	$107.1^{+7.8}_{-9.7}$	II	Konus-Wind	1	0.37 II	0.18 II
071020	0.87	2.1462	$85.0 \pm 6.9$	$1013^{+138}_{-107}$	II	Konus-Wind	1	1.71 II	1.84 II
071112C	2.9	0.8227	$11.8 \pm 1.9$	$740^{+326}_{-182}$	II	Konus-Wind	1	2.76 II	1.62 II
071117	0.97	1.3308	$37.6 \pm 3.1$	$648^{+235}_{-198}$	II	Konus-Wind	1	1.52 II	1.54 II
071227A	1.30	0.384	$0.591 \pm 0.025$	$875^{+190}_{-287}$	I+EE	Konus-Wind	1; 8	10.8 I	9.47 I
080123A	0.27	0.495	$3.20^{+6.59}_{-1.47}$	$2228^{+12723}_{-1308}$	I+EE	Konus-Wind	10; 15	14.0 I	26.9 I
080319B	23.0	0.9382	$1567 \pm 19$	$1264 \pm 17$	II+SNph	Konus-Wind	1; 2	0.67 II	0.14 II
080319C	3.5	1.9492	$155 \pm 16$	$1864^{+472}_{-353}$	II	Konus-Wind	1	2.48 II	1.33 II

**Table A1 – continued**

GRB	$T_{90,i}$ s	$z$	$E_{iso}$ $10^{51}$ erg	$E_{p,i}$ keV	Type	Experiment	Refs	$EH$ Type	$EHD$ Type
080411	21.1	1.0301	$238.5 \pm 7.7$	$540^{+43}_{-37}$	II	Konus-Wind	1	0.61 II	0.13 II
080413A	5.2	2.433	$72 \pm 12$	$659^{+381}_{-148}$	II	Konus-Wind	1	1.19 II	0.52 II
080413B	1.28	1.1014	$24 \pm 3$	$150 \pm 30$	II	Swift	3	0.42 II	0.37 II
080514B	2.04	$1.8^{+0.4}_{-0.3}$ PH	$286 \pm 13$	$549 \pm 34$	II	Konus-Wind	1	0.57 II	0.40 II
080602	23.0	1.8204	$80 \pm 14$	$1128^{+2084}_{-361}$	II	Konus-Wind	1	1.96 II	0.41 II
080603B	3.4	2.6892	$100 \pm 17$	$373^{+137}_{-66}$	II	Konus-Wind	1	0.59 II	0.32 II
080605	5.2	1.6403	$240.1 \pm 4.7$	$686^{+26}_{-24}$	II	Konus-Wind	1	0.77 II	0.34 II
080607	7.1	3.0363	$2171 \pm 60$	$1348^{+69}_{-65}$	II	Konus-Wind	1	0.62 II	0.23 II
080721	5.5	2.591	$1509 \pm 63$	$1760 \pm 147$	II	Konus-Wind	1	0.94 II	0.40 II
080804	10.6	2.2059	$115 \pm 20$	$810 \pm 45$	II	Swift	3; 12	1.21 II	0.37 II
080810	24.4	3.35	$450 \pm 50$	$1470 \pm 180$	II	Swift	3	1.28 II	0.26 II
080905A	0.86	0.122	$0.66 \pm 0.10$	$658^{+293}_{-123}$	I	Fermi	13	7.77 I	8.38 I
080913	1.04	6.695	$86 \pm 25$	$710 \pm 350$	II	Konus-Wind	3	1.20 II	1.17 II
080916A	3.9	0.6887	$8.49 \pm 0.70$	$218^{+30}_{-24}$	II	Konus-Wind	1	0.93 II	0.47 II
080916C	11.5	$4.35 \pm 0.15$ PH	$4820 \pm 390$	$2702^{+246}_{-230}$	II	Konus-Wind	1	0.91 II	0.27 II
081007	6.5	0.5295	$1.6 \pm 0.3$	$61 \pm 15$	II+SNsp	Swift	2; 3	0.51 II	0.20 II
081024B	0.16	3.05 PH	$24.4 \pm 2.2$	$5690^{+9060}_{-4321}$	I	Fermi	13	15.9 I	39.6 I
081028	64.4	3.038	$170 \pm 20$	$234 \pm 93$	II	Swift	3	0.30 II	0.04 II
081118	18.7	2.58	$43 \pm 9$	$147 \pm 14$	II	Swift	3	0.33 II	0.08 II
081121	5.5	2.512	$235.2 \pm 9.9$	$892^{+77}_{-63}$	II	Konus-Wind	1	1.00 II	0.43 II
081203A	96.4	2.05	$285 \pm 96$	$1336^{+1854}_{-497}$	II	Konus-Wind	1	1.39 II	0.14 II
081221	9.0	2.26	$397 \pm 10$	$264.1 \pm 6.5$	II	Konus-Wind	1	0.24 II	0.08 II
081222	3.2	2.77	$178 \pm 12$	$724^{+94}_{-72}$	II	Konus-Wind	1	0.91 II	0.51 II
090102	6.0	1.547	$200 \pm 10$	$1100^{+107}_{-92}$	II	Konus-Wind	1	1.32 II	0.54 II
090201	21.7	2.10	$955 \pm 28$	$484^{+22}_{-19}$	II	Konus-Wind	1	0.31 II	0.07 II
090227B	0.49	1.61 PH	$283 \pm 15$	$5116^{+392}_{-339}$	I	Fermi	13	5.35 I	7.64 I
090323	29.1	3.57	$5810 \pm 440$	$1906^{+206}_{-206}$	II	Konus-Wind	1	0.60 II	0.11 II
090328	30.4	0.736	$108.7 \pm 8.2$	$1297^{+187}_{-151}$	II	Konus-Wind	1	1.99 II	0.36 II
090418	21.5	1.608	$160 \pm 40$	$1567 \pm 384$	II	Swift	3	2.06 II	0.44 II
090423	1.13	8.1 PH	$110 \pm 30$	$491 \pm 200$	II	Swift	3	0.75 II	0.71 II
090424	2.8	0.544	$38.9 \pm 0.7$	$250.1 \pm 9.3$	II	Konus-Wind	1	0.58 II	0.35 II
090510A	0.51	0.903	$54.6 \pm 2.1$	$7955 \pm 343$	I	Fermi	1; 16	16.1 I	22.5 I
090516	41.1	4.109	$885 \pm 192$	$948^{+503}_{-217}$	II	Swift	3	0.63 II	0.10 II
090618	67.7	0.54	$252.9 \pm 4.9$	$288.0 \pm 9.2$	II+SNph	Konus-Wind	1; 2; 17	0.32 II	0.04 II
090709A	27.6	$1.8 \pm 0.6$ PH	$665 \pm 12$	$776 \pm 28$	II	Konus-Wind	1	0.58 II	0.11 II
090715B	17.8	3.0	$205 \pm 19$	$540^{+104}_{-76}$	II	Konus-Wind	1	0.64 II	0.15 II
090812	9.5	2.452	$271.8 \pm 9.7$	$1326^{+908}_{-362}$	II	Konus-Wind	1	1.41 II	0.46 II
090902B	6.9	1.822	$3050 \pm 20$	$2187 \pm 31$	II	Fermi	3	0.88 II	0.34 II
090926A	4.3	2.1062	$2111 \pm 53$	$1016 \pm 25$	II	Konus-Wind	1	0.48 II	0.23 II
090926B	49.0	1.24	$35.5 \pm 1.2$	$203.8 \pm 4.5$	II	Swift	3	0.49 II	0.07 II
091003A	10.6	0.8969	$106 \pm 1$	$922 \pm 45$	II	Fermi	3	1.43 II	0.44 II
091018	2.2	0.971	$8.0 \pm 0.9$	$55 \pm 26$	II	Konus-Wind	18; 19	0.24 II	0.16 II
091020	10.8	1.71	$122 \pm 24$	$130 \pm 19$	II	Swift	3	0.19 II	0.06 II
091024	52.5	1.092	$280 \pm 30$	$794 \pm 231$	II	Swift	3	0.83 II	0.12 II
091029	10.5	2.752	$74.0 \pm 7.4$	$230 \pm 66$	II	Swift	3	0.41 II	0.13 II
091117A	0.24	0.096	$0.0418 \pm 0.0058$	$711^{+238}_{-167}$	I	Konus-Wind	1	25.3 I	51.7 I
091127	3.3	0.49034	$16.3 \pm 0.2$	$53.6 \pm 3$	II+SNsp	Swift	2; 3	0.18 II	0.10 II
091208B	7.2	1.063	$20.1 \pm 0.7$	$297.5^{+37.1}_{-28.7}$	II	Swift	3	0.90 II	0.33 II
100117A	0.27	0.915	$7.8 \pm 1$	$547 \pm 84$	I	Fermi	13	2.41 II	4.63 I
100206A	0.09	0.408	$0.47 \pm 0.06$	$708 \pm 69$	I	Fermi	13	9.58 I	31.9 I
100414A	9.2	1.368	$766 \pm 12$	$1486 \pm 29$	II	Fermi	3	1.04 II	0.34 II
100418A	4.9	0.6239	$0.99 \pm 0.63$	$47.1 \pm 3.2$	II+SNph	Swift	2	0.47 II	0.21 II
100606A	23.1	1.5545	$294 \pm 23$	$2233^{+618}_{-411}$	II	Konus-Wind	1	2.30 II	0.48 II
100621A	30.0	0.542	$44.5 \pm 2.2$	$163^{+14}_{-12}$	II	Konus-Wind	1	0.36 II	0.07 II
100625A	0.13	0.452	$0.75 \pm 0.03$	$706 \pm 116$	I	Swift	13	7.92 I	22.0 I
100728A	62.3	1.567	$1140 \pm 68$	$783 \pm 41$	II	Konus-Wind	1	0.47 II	0.06 II
100728B	3.9	2.106	$26.6 \pm 1.1$	$407 \pm 47$	II	Swift	3	1.10 II	0.56 II
100814A	60.8	1.44	$75.9 \pm 5.8$	$312^{+32}_{-27}$	II	Konus-Wind	1	0.55 II	0.07 II
100816A	1.13	0.8049	$73 \pm 0.2$	$246.7 \pm 8.5$	II	Swift	3	0.44 II	0.42 II
100906A	33.1	1.727	$289 \pm 3$	$289^{+48}_{-55}$	II	Swift	3	0.30 II	0.05 II

**Table A1 – continued**

GRB	$T_{90,i}$ s	$z$	$E_{\text{iso}}$ $10^{51}$ erg	$E_{\text{p},i}$ keV	Type	Experiment	Refs	<i>EH</i> Type	<i>EHD</i> Type
101213A	21.6	0.414	$5.4 \pm 0.4$	$354^{+58}_{-42}$	II	Konus-Wind	<a href="#">1</a>	1.80 II	0.39 II
101219A	0.30	0.718	$6.51 \pm 0.36$	$1014^{+110}_{-96}$	I	Konus-Wind	<a href="#">1</a>	4.79 I	8.75 I
101219B	21.9	0.55	$5.9 \pm 0.4$	$109 \pm 12$	II+SNsp	Swift	<a href="#">2; 3</a>	0.54 II	0.12 II
101225A	3790	0.847	$12 \pm 3$	$70 \pm 37$	II+SNph	Swift	<a href="#">2</a>	0.26 II	0.004 II
110205A	79.8	2.22	$560 \pm 60$	$715 \pm 239$	II	Swift	<a href="#">3</a>	0.57 II	0.06 II
110213A	11.9	1.46	$69 \pm 2$	$242^{+21}_{-17}$	II	Swift	<a href="#">3</a>	0.45 II	0.13 II
110213B*	24.0	1.083	$70.4 \pm 5$	$256 \pm 40$	II	Konus-Wind	<a href="#">20; 21</a>	0.47 II	0.10 II
110402A	2.8	0.805	$15.2 \pm 2.9$	$1924^{+767}_{-451}$	I+EE	Fermi	<a href="#">22</a>	6.48 I	3.87 I
110422A	8.1	1.77	$747 \pm 11$	$429.4 \pm 8.3$	II	Konus-Wind	<a href="#">1</a>	0.30 II	0.11 II
110503A	2.6	1.613	$212.8 \pm 9.5$	$575 \pm 31$	II	Konus-Wind	<a href="#">1</a>	0.67 II	0.42 II
110715A	1.56	0.82	$49.7 \pm 3.3$	$217 \pm 13$	II	Konus-Wind	<a href="#">1</a>	0.46 II	0.36 II
110731A	1.75	2.83	$315 \pm 12$	$1103^{+69}_{-61}$	II	Konus-Wind	<a href="#">1</a>	1.11 II	0.84 II
110918A	9.9	0.984	$2705 \pm 99$	$667^{+79}_{-69}$	II	Konus-Wind	<a href="#">1</a>	0.28 II	0.09 II
111008A	2.1	5.0	$414 \pm 71$	$624^{+186}_{-120}$	II	Konus-Wind	<a href="#">1</a>	0.56 II	0.39 II
111117A*	0.18	2.211	$8.9 \pm 3.4$	$1350 \pm 450$	I	Fermi	<a href="#">13; 23</a>	5.63 I	13.3 I
111209A	5963	0.677	$52 \pm 10$	$520 \pm 89$	II+SNsp	Swift	<a href="#">2</a>	1.07 II	0.014 II
111228A	29.5	0.7156	$16.5 \pm 4$	$74^{+31}_{-53}$	II+SNph	Konus-Wind	<a href="#">1; 2</a>	0.24 II	0.04 II
120119A	14.5	1.728	$402 \pm 28$	$417 \pm 33$	II	Konus-Wind	<a href="#">1</a>	0.38 II	0.10 II
120326A*	24.9	1.798	$38.2 \pm 4.1$	$115 \pm 19$	II	Swift	<a href="#">24; 25</a>	0.27 II	0.05 II
120624B	83.8	2.1974	$2820 \pm 12$	$1791^{+157}_{-134}$	II	Konus-Wind	<a href="#">1</a>	0.75 II	0.08 II
120711A	17.2	1.405	$2037 \pm 46$	$2552^{+91}_{-87}$	II	Konus-Wind	<a href="#">1</a>	1.21 II	0.29 II
120712A*	4.3	4.1745	$151.7 \pm 1.7$	$642 \pm 134.5$	II	Fermi	<a href="#">26; 27</a>	0.86 II	0.42 II
120716A	59.8	2.486	$264 \pm 25$	$662^{+174}_{-105}$	II	Konus-Wind	<a href="#">1</a>	0.71 II	0.09 II
120724A*	29.4	1.48	$6.02 \pm 1.09$	$68.4 \pm 18.6$	II	Swift	<a href="#">28; 29</a>	0.33 II	0.06 II
120729A	39.7	0.80	$23 \pm 15$	$559 \pm 57$	II+SNph	Fermi	<a href="#">2; 30</a>	1.60 II	0.25 II
120804A	0.33	1.3 PH	$6.57 \pm 0.47$	$283^{+62}_{-41}$	II	Konus-Wind	<a href="#">1</a>	1.33 II	2.32 II
120811C*	7.3	2.671	$88.1 \pm 8.3$	$157 \pm 21$	II	Swift	<a href="#">31; 32</a>	0.26 II	0.10 II
120909A	23.3	3.93	$690 \pm 50$	$1652 \pm 123$	II	Konus-Wind	<a href="#">33</a>	1.21 II	0.25 II
120922A*	44.5	$3.1 \pm 0.2$ PH	$252.5 \pm 4.9$	$247 \pm 26$	II	Fermi	<a href="#">34; 35</a>	0.27 II	0.04 II
121128A	3.1	2.2	$100.6 \pm 3.6$	$246 \pm 10$	II	Konus-Wind	<a href="#">1</a>	0.39 II	0.22 II
130215A	90.0	0.597	$56.0 \pm 1.4$	$248 \pm 101$	II+SNsp	Fermi	<a href="#">2; 30; 36; 37</a>	0.50 II	0.05 II
130408A	0.89	3.758	$324 \pm 61$	$1289^{+176}_{-205}$	II	Konus-Wind	<a href="#">1</a>	1.28 II	1.35 II
130420A*	45.70	1.297	$62.9 \pm 1.1$	$130.8 \pm 7.0$	II	Fermi	<a href="#">34; 38</a>	0.25 II	0.04 II
130427A	46.1	0.3399	$890.4 \pm 4.6$	$1415 \pm 13$	II+SNsp	Konus-Wind	<a href="#">1; 2</a>	0.94 II	0.14 II
130505A	4.5	2.27	$4380 \pm 100$	$1939^{+85}_{-78}$	II	Konus-Wind	<a href="#">1</a>	0.68 II	0.32 II
130514A	34.8	$3.6 \pm 0.2$ PH	$495^{+85}_{-67}$	$506^{+193}_{-97}$	II	Konus-Wind	<a href="#">39</a>	0.42 II	0.07 II
130518A	8.2	2.488	$2160 \pm 140$	$1158^{+188}_{-157}$	II	Konus-Wind	<a href="#">1</a>	0.54 II	0.19 II
130603B	0.16	0.356	$1.96 \pm 0.10$	$823^{+83}_{-71}$	I	Konus-Wind	<a href="#">1</a>	6.29 I	15.7 I
130606A	1.74	5.913	$283 \pm 52$	$2032^{+622}_{-346}$	II	Konus-Wind	<a href="#">40</a>	2.12 II	1.61 II
130610A*	7.0	2.092	$57.82 \pm 0.65$	$895 \pm 382$	II	Fermi	<a href="#">34; 41</a>	1.77 II	0.67 II
130612A*	1.9	2.006	$7.19 \pm 0.80$	$186 \pm 32$	II	Fermi	<a href="#">42; 43</a>	0.85 II	0.61 II
130701A	1.70	1.155	$26.2 \pm 1.0$	$191.8 \pm 8.6$	II	Konus-Wind	<a href="#">1</a>	0.52 II	0.40 II
130702A	51.4	0.145	$0.64 \pm 0.13$	$17.2 \pm 5.7$	II+SNsp	Swift	<a href="#">2; 44</a>	0.21 II	0.03 II
130831A	11.9	0.4791	$8.05 \pm 0.57$	$79.9^{+10.4}_{-13.3}$	II+SNsp	Konus-Wind	<a href="#">1; 2; 30</a>	0.35 II	0.10 II
130907A	80.6	1.238	$3849 \pm 130$	$866 \pm 36$	II	Konus-Wind	<a href="#">1</a>	0.32 II	0.04 II
130925A	3341	0.347	$150 \pm 3$	$244 \pm 13$	II	Konus-Wind	<a href="#">45</a>	0.33 II	0.006 II
131004A	0.90	0.71	$0.69 \pm 0.03$	$202 \pm 51$	I	Fermi	<a href="#">14</a>	2.35 II	2.48 II
131011A*	26.8	1.874	$83.4 \pm 0.6$	$788 \pm 71$	II	Fermi	<a href="#">34; 46</a>	1.34 II	0.26 II
131030A	6.9	1.293	$327 \pm 13$	$449 \pm 14$	II	Konus-Wind	<a href="#">1</a>	0.44 II	0.17 II
131105A	41.3	1.686	$153 \pm 12$	$540^{+107}_{-70}$	II	Konus-Wind	<a href="#">1</a>	0.72 II	0.11 II
131108A	5.2	2.40	$540 \pm 24$	$1217^{+105}_{-88}$	II	Konus-Wind	<a href="#">1</a>	0.98 II	0.43 II
131117A*	2.2	4.042	$10.3 \pm 1.8$	$222 \pm 37$	II	Swift	<a href="#">47; 48</a>	0.87 II	0.59 II
131231A	17.7	0.6439	$211 \pm 6$	$266 \pm 10$	II	Konus-Wind	<a href="#">1</a>	0.31 II	0.07 II
140206A*	39.3	2.73	$2778 \pm 5$	$1780 \pm 120$	II	Fermi	<a href="#">34; 49</a>	0.75 II	0.12 II
140213A	7.4	1.2076	$88.8 \pm 2.4$	$220.8 \pm 8.8$	II	Konus-Wind	<a href="#">1</a>	0.37 II	0.14 II
140226A*	5.0	1.98	$56.8 \pm 10.8$	$1234 \pm 235$	II	Konus-Wind	<a href="#">50; 51</a>	2.45 II	1.10 II
140304A	5.1	5.283	$103 \pm 10$	$863^{+111}_{-99}$	II	Swift	<a href="#">52; 53</a>	1.35 II	0.60 II
140419A	10.8	3.956	$2280 \pm 180$	$2161^{+243}_{-198}$	II	Konus-Wind	<a href="#">1</a>	0.98 II	0.30 II
140423A*	22.3	3.26	$438 \pm 3$	$517 \pm 65$	II	Fermi	<a href="#">34; 54</a>	0.45 II	0.10 II
140506A	32.3	0.889	$14.0 \pm 1.4$	$378^{+170}_{-79}$	II	Konus-Wind	<a href="#">1</a>	1.32 II	0.23 II

**Table A1 – continued**

GRB	$T_{90,i}$ s	$z$	$E_{iso}$ $10^{51}$ erg	$E_{p,i}$ keV	Type	Experiment	Refs	$EH$ Type	$EHD$ Type
140508A	73.8	1.027	$225 \pm 15$	$446^{+28}_{-26}$	II	Konus-Wind	1	0.51 II	0.06 II
140512A	81.8	0.725	$72.5 \pm 6.1$	$826^{+202}_{-136}$	II	Konus-Wind	1	1.49 II	0.17 II
140515A*	3.2	6.32	$53.8 \pm 5.8$	$376 \pm 108$	II	Swift	55; 56	0.76 II	0.43 II
140518A*	10.6	4.707	$59.8 \pm 5.8$	$251 \pm 43$	II	Swift	57; 58	0.49 II	0.15 II
140606B	4.9	0.384	$2.5 \pm 0.2$	$352^{+46}_{-37}$	II+SNsp	Konus-Wind	2; 59	2.44 II	1.10 II
140619B	0.14	2.67	$26.4 \pm 1.2$	$4844 \pm 1068$	I	Fermi	14	13.07 I	35.42 I
140620A*	15.1	2.04	$72.75 \pm 0.66$	$387 \pm 34$	II	Fermi	34; 60	0.70 II	0.18 II
140622A	0.07	0.959	$0.10 \pm 0.02$	$86.2 \pm 15.7$	I	Swift	61	2.17 II	8.18 I
140623A*	38.0	1.92	$35.32 \pm 0.44$	$834 \pm 317$	II	Fermi	34; 62	2.00 II	0.33 II
140629A	7.9	2.275	$44.0 \pm 6.5$	$282 \pm 56$	II	Konus-Wind	63	0.62 II	0.22 II
140703A*	20.3	3.14	$183.5 \pm 1.1$	$913 \pm 110$	II	Fermi	34; 64	1.14 II	0.25 II
140801A	2.7	1.32	$55.5 \pm 1.3$	$250.6 \pm 7.0$	II	Konus-Wind	1	0.50 II	0.31 II
140808A	1.21	3.293	$84.8 \pm 5.1$	$537^{+60}_{-47}$	II	Konus-Wind	1	0.91 II	0.83 II
140903A	0.22	0.351	$0.044 \pm 0.003$	$60 \pm 22$	I	Swift	14	2.08 II	4.41 I
140907A*	16.2	1.21	$27.10 \pm 0.25$	$313 \pm 21$	II	Fermi	34; 65	0.84 II	0.21 II
141004A	1.91	0.573	$2.10 \pm 0.22$	$231 \pm 44$	II+SNph	Fermi	66; 67	1.72 II	1.24 II
141028A*	9.5	2.33	$509.5 \pm 1.2$	$980 \pm 53$	II	Fermi	34; 68	0.81 II	0.26 II
141109A	23.5	2.993	$331.0^{+78}_{-59}$	$763^{+303}_{-172}$	II	Konus-Wind	69	0.75 II	0.16 II
141212A	0.19	0.596	$0.068 \pm 0.011$	$151 \pm 14$	I	Swift	14	4.45 I	10.26 I
141220A	3.0	1.3195	$22.9 \pm 1.2$	$322^{+23}_{-21}$	II	Konus-Wind	1	0.92 II	0.53 II
141221A*	9.7	1.452	$24.57 \pm 0.35$	$446 \pm 85$	II	Fermi	34; 70	1.24 II	0.40 II
141225A*	29.4	0.915	$8.59 \pm 0.08$	$343 \pm 52$	II	Fermi	34; 71	1.45 II	0.27 II
150101B	0.02	0.093	$0.0022 \pm 0.0003$	$34 \pm 23$	I	Fermi	14	3.91 I	28.89 I
150120A*	0.8	0.46	$0.19 \pm 0.04$	$190^{+220}_{-73}$	I	Fermi	72; 73	3.69 I	4.13 I
150206A	11.4	2.087	$619 \pm 45$	$704^{+71}_{-68}$	II	Konus-Wind	1	0.54 II	0.16 II
150301B*	5.3	1.5169	$19.94 \pm 0.18$	$568 \pm 74$	II	Fermi	34; 74	1.72 II	0.75 II
150314A	3.7	1.758	$768 \pm 21$	$965 \pm 28$	II	Konus-Wind	1	0.68 II	0.35 II
150323A	96.2	0.593	$12.56 \pm 0.69$	$151^{+14}_{-13}$	II	Konus-Wind	1	0.55 II	0.06 II
150403A	6.9	2.06	$1164 \pm 62$	$1141^{+104}_{-95}$	II	Konus-Wind	1	0.68 II	0.26 II
150413A	63.7	3.139	$653^{+162}_{-129}$	$397^{+232}_{-91}$	II	Konus-Wind	75	0.30 II	0.04 II
150423A	1.14	0.22	$0.0075 \pm 0.0013$	$146 \pm 43$	I	Swift	14	10.38 I	9.73 I
150424A	0.21	0.30	$4.34 \pm 0.16$	$1191^{+64}_{-61}$	I+EE	Konus-Wind	1; 76	6.62 I	14.4 I
150514A	1.09	0.807	$8.78^{+0.78}_{-0.78}$	$108^{+11}_{-13}$	II	Konus-Wind	1	0.45 II	0.43 II
150727A*	37.6	0.313	$2.00 \pm 0.11$	$323^{+47}_{-32}$	II	Fermi	34; 77	2.45 II	0.40 II
150818A	36.7	0.282	$1.00^{+0.15}_{-0.13}$	$128^{+37}_{-23}$	II+SNsp	Konus-Wind	2; 78; 79	1.28 II	0.21 II
150821A	63.2	0.755	$155 \pm 12$	$765^{+188}_{-126}$	II	Konus-Wind	1	1.02 II	0.13 II
151021A	17.1	2.33	$1127 \pm 94$	$566^{+43}_{-37}$	II	Konus-Wind	1	0.34 II	0.08 II
151027A	64.8	0.81	$33 \pm 4.1$	$313^{+105}_{-58}$	II	Konus-Wind	1	0.77 II	0.10 II
151029A*	3.7	1.423	$2.88 \pm 0.37$	$82 \pm 17$	II	Swift	80; 81	0.54 II	0.28 II
151111A*	17.1	$3.5 \pm 0.3$ PH	$58.5 \pm 3.5$	$255 \pm 41$	II	Swift	82; 83	0.50 II	0.12 II
160131A	55.7	0.972	$870 \pm 66$	$1284^{+454}_{-308}$	II	Konus-Wind	1	0.86 II	0.12 II
160227A*	93.6	2.38	$55.6 \pm 3.6$	$222 \pm 55$	II	Swift	84; 85	0.45 II	0.05 II
160410A	0.58	1.717	$93 \pm 18$	$3853^{+1429}_{-973}$	I+EE	Konus-Wind	1; 86	6.29 I	8.26 I
160509A	13.1	1.17	$1130 \pm 100$	$625^{+63}_{-59}$	II	Konus-Wind	1	0.38 II	0.10 II
160623A	15.8	0.367	$253.0 \pm 3.4$	$755 \pm 19$	II	Konus-Wind	1	0.83 II	0.21 II
160624A	0.13	0.483	$0.40^{+0.14}_{-0.15}$	$1247 \pm 531$	I	Fermi	13	18.0 I	49.9 I
160625B	8.7	1.406	$5101 \pm 62$	$1374^{+29}_{-26}$	II	Konus-Wind	1; 87	0.45 II	0.15 II
160629A	14.9	3.332	$389 \pm 14$	$1022^{+93}_{-82}$	II	Konus-Wind	1	0.94 II	0.24 II
160804A*	75.8	0.736	$26.95 \pm 0.36$	$131.7 \pm 4.9$	II	Fermi	34; 88	0.35 II	0.04 II
160821B	0.41	0.16	$0.12 \pm 0.02$	$97.4 \pm 22.0$	I	Fermi	13	2.28 II	3.55 I
161014A	6.5	2.823	$82 \pm 12$	$864^{+1021}_{-302}$	II	Konus-Wind	89	1.48 II	0.58 II
161017A	10.0	2.013	$83 \pm 11$	$871 \pm 220$	II	Konus-Wind	90	1.49 II	0.47 II
161023A	13.5	2.708	$680 \pm 97$	$604^{+137}_{-104}$	II	Konus-Wind	91	0.45 II	0.12 II
161117A	51.0	1.549	$130.0 \pm 7.6$	$176^{+15}_{-18}$	II	Konus-Wind	92	0.25 II	0.04 II
161129A*	21.9	0.645	$7.83 \pm 0.06$	$352 \pm 37$	II	Fermi	34; 93	1.55 II	0.33 II
161219B	6.1	0.1475	$0.116 \pm 0.008$	$71.0 \pm 19.3$	II+SNsp	Swift	94; 95; 96	1.68 II	0.68 II
170113A*	7.0	1.968	$9.24 \pm 0.97$	$218 \pm 100$	II	Swift	97; 98	0.90 II	0.34 II
170202A	6.5	3.645	$170 \pm 40$	$1147^{+771}_{-399}$	II	Konus-Wind	99	1.47 II	0.58 II
170214A*	34.8	2.53	$3184.3 \pm 2.1$	$1810 \pm 34$	II	Fermi	34; 100	0.72 II	0.12 II
170428A	0.14	0.454	$1.86^{+0.32}_{-0.98}$	$1428^{+346}_{-313}$	I	Konus-Wind	13	11.1 I	29.8 I

**Table A1 – continued**

GRB	$T_{90,i}$ s	$z$	$E_{\text{iso}}$ $10^{51}$ erg	$E_{\text{p},i}$ keV	Type	Experiment	Refs	$EH$ Type	$EHD$ Type
170604A	12.9	1.329	$47 \pm 6$	$512^{+168}_{-112}$	II	Konus-Wind	101	1.10 II	0.31 II
170607A*	14.5	0.557	$9.15 \pm 0.05$	$226 \pm 18$	II	Fermi	34; 102	0.93 II	0.25 II
170705A*	7.6	2.010	$180 \pm 20$	$467^{+93}_{-66}$	II	Fermi	34; 103; 104	0.59 II	0.21 II
170817A	0.50	0.00968	$(4.7 \pm 0.7) \times 10^{-5}$	$65.6^{+35.3}_{-14.1}$	I	Fermi	105	35.3 I	50.0 I
170903A*	13.6	0.886	$8.65 \pm 0.06$	$180 \pm 25$	II	Fermi	34; 106	0.76 II	0.21 II
171010A	116.7	0.3285	$180 \pm 5.5$	$227.2^{+9.3}_{-8.0}$	II+SNsp	Konus-Wind	107; 108	0.29 II	0.03 II
171205A	183.7	0.0368	$0.0218^{+0.0063}_{-0.0050}$	$125^{+141}_{-37}{}^0$	II+SNsp	Konus-Wind	109; 110	5.78 I	0.43 II
171222A*	23.6	2.409	$89.4 \pm 1.3$	$694 \pm 12$	II	Fermi	34; 111	1.15 II	0.24 II
180205A*	6.4	1.409	$9.72 \pm 0.78$	$205 \pm 34$	II	Fermi	34; 112; 113	0.83 II	0.33 II
180325A	3.1	2.248	$230 \pm 36$	$994^{+162}_{-127}$	II	Konus-Wind	114	1.13 II	0.64 II
180329B*	70.0	1.998	$46.9 \pm 4.3$	$146 \pm 28$	II	Swift	115; 116	0.31 II	0.04 II
180620B*	22.1	1.1175	$30.4 \pm 0.3$	$372 \pm 105$	II	Fermi	34; 117	0.95 II	0.20 II
180720B*	29.6	0.654	$339.7 \pm 0.1$	$1052 \pm 26$	II	Fermi	34; 118	1.02 II	0.19 II
180728A	15.5	0.117	$2.33 \pm 0.10$	$108^{+8}_{-7}$	II	Konus-Wind	119	0.77 II	0.20 II
180914B*	130	1.096	$3700 \pm 161$	$977^{+61}_{-57}$	II	Konus-Wind	120; 121	0.37 II	0.03 II
181020A	6.6	2.938	$828^{+116}_{-107}$	$1461^{+225}_{-205}$	II	Konus-Wind	122	0.99 II	0.39 II
181110A	28	1.505	$110 \pm 20$	$120^{+35}_{-68}$	II	Konus-Wind	123	0.18 II	0.04 II
181201A	120	0.450	$100 \pm 5$	$220 \pm 9$	II+SNph	Konus-Wind	124; 125; 126; 127	0.35 II	0.03 II
190106A	27.6	1.859	$99.6^{+22.5}_{-15.5}$	$489^{+257}_{-120}$	II	Konus-Wind	128	0.78 II	0.15 II
190114C	120	0.4245	$270.3 \pm 2.4$	$929.3 \pm 9.4$	II+SNsp	Fermi	129; 130; 131	0.99 II	0.09 II

\*  $E_{\text{iso}}$  and  $E_{\text{p},i}$  values are calculated in the paper.

<sup>a</sup> For the ‘I+EE’ GRBs the duration of an initial pulse complex is presented.

<sup>b</sup> PH is for photometrical redshift.

<sup>c</sup> The classification of the burst, taken from the literature. ‘I’ – regular type I GRBs, ‘I+EE’ – type I GRBs with an extended emission, ‘II’ – regular type II GRBs, ‘II+SNsp’ – type II GRBs with spectroscopically confirmed Ic supernova, ‘II+SNph’ – type II GRBs with photometrically confirmed Ic supernova.

<sup>d</sup> The experiment, used for the calculation of  $T_{90,i}$ ,  $E_{\text{p},i}$  and  $E_{\text{iso}}$  values.

<sup>e</sup> 1 – Tsvetkova et al. (2017), 2 – Cano et al. (2017), 3 – Qin & Chen (2013), 4 – Amati (2006), 5 – Frontera et al. (2009), 6 – Minaev et al. (2014), 7 – Zhang et al. (2009), 8 – Norris et al. (2010), 9 – Volnova et al. (2014), 10 – Svinkin et al. (2016a), 11 – Butler et al. (2007), 12 – Krühler et al. (2015), 13 – Zou et al. (2018), 14 – Zhang et al. (2018b), 15 – Tueller et al. (2008), 16 – Minaev & Pozanenko (2017), 17 – Cano et al. (2011), 18 – Nava et al. (2012), 19 – Markwardt et al. (2009), 20 – Golenetskii et al. (2011), 21 – Cenko et al. (2011), 22 – Pozanenko (2019), 23 – Selsing et al. (2018), 24 – Barthelmy et al. (2012), 25 – Tello et al. (2012), 26 – Gruber (2012), 27 – Xu et al. (2012), 28 – Krimm et al. (2012a), 29 – Cucchiara et al. (2012), 30 – Cano et al. (2014), 31 – Krimm et al. (2012b), 32 – Thoene et al. (2012), 33 – Golenetskii et al. (2012), 34 – Narayana Bhat et al. (2016), 35 – Knust et al. (2012), 36 – Younes & Bhat (2013), 37 – Cucchiara & Fumagalli (2013), 38 – de Ugarte Postigo et al. (2013), 39 – Pal'Shin et al. (2013), 40 – Golenetskii et al. (2013a), 41 – Smette et al. (2013), 42 – Fitzpatrick (2013), 43 – Tanvir et al. (2013), 45 – Golenetskii et al. (2013b), 46 – Rau et al. (2013), 47 – Krimm et al. (2013), 48 – Hartoog et al. (2013), 49 – Malesani et al. (2014), 50 – Golenetskii et al. (2014a), 51 – Cenko et al. (2014), 52 – Jeong et al. (2014), 53 – Jenke & Fitzpatrick (2014), 54 – Tanvir et al. (2014), 55 – Stamatikos et al. (2014), 56 – Chornock et al. (2014a), 57 – Ukwatta et al. (2014), 58 – Chornock et al. (2014b), 59 – Golenetskii et al. (2014b), 60 – Kasliwal et al. (2014), 61 – Pandey et al. (2019), 62 – Bhalerao et al. (2014), 63 – Golenetskii et al. (2014c), 64 – Castro-Tirado et al. (2014a), 65 – Castro-Tirado et al. (2014b), 66 – Pelassa (2014), 67 – de Ugarte Postigo et al. (2014), 68 – Xu et al. (2014), 69 – Golenetskii et al. (2014d), 70 – Perley et al. (2014), 71 – Gorosabel et al. (2014), 72 – von Kienlin & Burns (2015), 73 – Chornock & Fong (2015), 74 – de Ugarte Postigo et al. (2015), 75 – Golenetskii et al. (2015a), 76 – Norris et al. (2015), 77 – Tanvir et al. (2015a), 78 – Golenetskii et al. (2015b), 79 – Mazaeva et al. (2015), 80 – Stamatikos et al. (2015), 81 – Tanvir et al. (2015b), 82 – Bolmer et al. (2015), 83 – Cummings et al. (2015), 84 – Xu et al. (2016a), 85 – Sakamoto et al. (2016a), 86 – Sakamoto et al. (2016b), 87 – Zhang et al. (2018a), 88 – Xu et al. (2016b), 89 – Frederiks et al. (2016a), 90 – Frederiks et al. (2016b), 91 – Frederiks et al. (2016c), 92 – Svinkin et al. (2016b), 93 – Cano et al. (2016), 94 – Palmer et al. (2016), 95 – Tanvir et al. (2016), 96 – de Ugarte Postigo et al. (2016), 97 – Markwardt et al. (2017), 98 – Xu et al. (2017), 99 – Frederiks et al. (2017a), 100 – Kruehler et al. (2017), 101 – Frederiks et al. (2017b), 102 – de Ugarte Postigo et al. (2017a), 103 – de Ugarte Postigo et al. (2017b), 104 – Svinkin et al. (2017), 105 – Pozanenko et al. (2018), 106 – de Ugarte Postigo et al. (2017c), 107 – Frederiks et al. (2017c), 108 – de Ugarte Postigo et al. (2017d), 109 – D'Elia et al. (2018), 110 – de Ugarte Postigo et al. (2017e), 111 – de Ugarte Postigo et al. (2017f), 112 – Tanvir et al. (2018), 113 – von Kienlin (2018), 114 – Frederiks et al. (2018a), 115 – Palmer et al. (2018), 116 – Izzo et al. (2018a), 117 – Izzo et al. (2018b), 118 – Vreeswijk et al. (2018), 119 – Frederiks et al. (2018b), 120 – Frederiks et al. (2018c), 121 – D'Avanzo et al. (2018), 122 – Tsvetkova et al. (2018), 123 – Frederiks et al. (2018d), 124 – Izzo et al. (2018c), 125 – Svinkin et al. (2018), 126 – Belkin et al. (2019b), 127 – Belkin et al. (2019a), 128 – Tsvetkova et al. (2019), 129 – Castro-Tirado et al. (2019), 130 – Melandri et al. (2019), 131 – Pozanenko et al. (2019)

<sup>f</sup> The value of the parameter  $EH$  and corresponding GRB type, obtained from the blind  $EH$ -based classification.

<sup>g</sup> The value of the parameter  $EHD$  and corresponding GRB type, obtained from the blind  $EHD$ -based classification.